

Molecular Interaction between the Chaperone Hsc70 and the N-terminal Flank of Huntingtin Exon 1 Modulates Aggregation*

Received for publication, August 26, 2014, and in revised form, November 18, 2014. Published, JBC Papers in Press, December 10, 2014, DOI 10.1074/jbc.M114.603332

Elodie Monsellier¹, Virginie Redeker, Gemma Ruiz-Arlandis, Luc Bousset, and Ronald Melki²

From the Neuroscience Paris-Saclay Institute, CNRS, Avenue de la Terrasse, 91198 Gif-sur-Yvette, France

Background: Hsc70 has an alleviating effect on the toxicity of polyglutamine (polyQ)-containing proteins *in vivo*.

Results: Hsc70 binds specifically to the N-terminal flank of huntingtin exon 1.

Conclusion: Hsc70 interaction with huntingtin exon 1 N-terminal flank affects the conformation of the resulting assemblies.

Significance: We identify the surface interfaces between Hsc70 and huntingtin exon 1, which allows the design of future therapeutic tools.

The aggregation of polyglutamine (polyQ)-containing proteins is at the origin of nine neurodegenerative diseases. Molecular chaperones prevent the aggregation of polyQ-containing proteins. The exact mechanism by which they interact with polyQ-containing, aggregation-prone proteins and interfere with their assembly is unknown. Here we dissect the mechanism of interaction between a huntingtin exon 1 fragment of increasing polyQ lengths (HttEx1Qn), the aggregation of which is tightly associated with Huntington's disease, and molecular chaperone Hsc70. We show that Hsc70, together with its Hsp40 co-chaperones, inhibits HttEx1Qn aggregation and modifies the structural, seeding, and infectious properties of the resulting fibrils in a polyQ-independent manner. We demonstrate that Hsc70 binds the 17-residue-long N-terminal flank of HttEx1Qn, and we map Hsc70-HttEx1Qn surface interfaces at the residue level. Finally, we show that this interaction competes with homotypic interactions between the N termini of different HttEx1Qn molecules that trigger the aggregation process. Our results lay the foundations of future therapeutic strategies targeting huntingtin aggregation in Huntington disease.

Huntington disease (HD)³ is a dominant heritable neurodegenerative disease tightly associated with the aggregation of the protein huntingtin (Htt), a large protein of ~3144 residues generated through the expression of the 67 exons of the *HTT* gene or a proteolytic N-terminal fragment of Htt corresponding to

exon 1 (HttEx1Qn) (1–3). Htt plays critical roles in early development, in the regulation of gene transcription, in neurogenesis and cell survival, and in axonal transport (4). The aggregation of Htt and HttEx1Qn occurs in individuals bearing an abnormally long homopolymeric tract of glutamine residues (polyQ) in the N-terminal part of Htt above a threshold of ~35Q due to the expansion of CAG tracts within the protein-coding region of the *HTT* gene (5, 6). HttEx1Qn with the expanded polyQ tract ($n > 35$) aggregates in animal models for HD and *in vitro* into insoluble β -sheet-rich fibrillar assemblies (7, 8) that have prion-like properties (9, 10).

Synthetic and recombinant peptides made of 35 or more glutamines assemble in a nucleation-dependent manner into fibrils resembling those of HttEx1Qn with similar polyQ lengths (11). However, because the polyQ stretch is flanked N- and C-terminally by 17 and 52 amino acid residues, respectively, with the C-terminal flank comprising two stretches of 11 and 10 proline residues separated by a 17-amino acid stretch mostly made of Gln and Pro residues, studies aimed at documenting the way the polyQ context within HttEx1Qn (*e.g.* HttEx1Qn flanks) affects aggregation have been performed. Whereas the C-terminal Pro-rich polyQ flank has been repeatedly shown to negatively affect aggregation (12), two models have been proposed to account for the role of the polyQ 17-residue-long N-terminal flank (Nt₁₇) in HttEx1Qn aggregation (13, 14).

Molecular chaperones combat protein aggregation within the cells. The roles of various molecular chaperones in polyQ-containing protein aggregation have been subject to active investigations, but their modes of action remain elusive. Various and sometimes contradictory effects have been reported in cellular or animal models (15–19). In addition, the existence of a direct interaction between the chaperones and the polyQ stretch *per se* is subject to debate (19–22) because the interaction between the chaperones and the hydrophilic polyQ stretch is *a priori* unfavorable (23, 24).

Here we assess the role and mechanism of action of the constitutively expressed heat shock protein Hsc70 and its co-chaperones from the Hsp40 family in HttEx1Qn aggregation. We show that Hsc70, in its active, functional form, affects HttEx1Qn assembly by interacting with Nt₁₇ in a manner inde-

* This work was supported by Agence Nationale de la Recherche Grant ANR-11-BSV8-021-01, CNRS, the Human Frontier Science Program, the European Community's Seventh Framework Program FP7/2010, Marie Curie Actions Grant 264508, and a "Coup d'Élan à la Recherche Française" award from Fondation Bettencourt-Schueller.

R. M. dedicates this work to the late Professor Paul Cohen.

¹ To whom correspondence may be addressed. Tel.: 33-16982-3486; E-mail: monsellier@lebs.cnrs-gif.fr.

² To whom correspondence may be addressed. Tel.: 33-16982-3503; E-mail: melki@lebs.cnrs-gif.fr.

³ The abbreviations used are: HD, Huntington disease; polyQ, polyglutamine; Hsc, constitutive heat-shock protein; Htt, huntingtin; HttEx1Qn, huntingtin exon 1 with a polyQ length of n ; Nt₁₇, 17-residue-long N-terminal flank of HttEx1Qn; BS3, bis(sulfosuccinimidyl) suberate; ChFP, mCherry fluorescent protein; MBP, maltose-binding protein; TEV, tobacco etch virus; nanoLC, nanoliquid chromatography.

pendent of the polyQ stretch. We show that the fibrillar scaffold and *in vivo* seeding properties of HttEx1Qn fibrils assembled in the presence of Hsc70 are distinct from those of HttEx1Qn fibrils assembled in the absence of Hsc70. Using chemical cross-linking with the homobifunctional NHS-ester BS3, we provide evidence for an Hsc70-HttEx1Qn complex. We map the surface interface between Hsc70 and HttEx1Qn after identification of the cross-linked polypeptides by mass spectrometry analyses.

Our results highlight the importance of the Htt exon 1 N-terminal flank in the assembly process of HttEx1Qn. Using the same cross-linking strategy as above, we demonstrate Nt₁₇-Nt₁₇ interaction in the early stages of HttEx1Qn coalescence during assembly into fibrils. Identification of the cross-linked polypeptides, together with the fact that Nt₁₇ is α -helical, leads us to propose a model for on-assembly pathway oligomeric HttEx1Qn species that integrates structural constraints.

EXPERIMENTAL PROCEDURES

Expression and Purification of Recombinant Polypeptides and Synthetic Nt₁₇ Peptides—Recombinant C-terminally His₆-tagged MBP-TEV-HttEx1Qn-His with various polyQ lengths ($n = 17, 25, 30, 35, 41, \text{ or } 48$) was expressed in *Escherichia coli* strain BL21(DE3) (Stratagene, Santa Clara, CA) and purified in two steps. The protein lysate was first loaded onto a 10-ml bed volume amylose resin column (New England Biolabs) equilibrated in 20 mM Tris-HCl, pH 7.5, 150 mM KCl, 10% glycerol, 1 mM 2- β -mercaptoethanol. The MBP-TEV-HttEx1Qn-His was eluted from this column with 10 mM maltose, and its concentration was determined from its absorbance at 280 nm using an extinction coefficient of 67,840 M⁻¹ cm⁻¹ for all of the polyQ lengths. MBP-TEV protease, produced using the plasmid pRK1043 (Addgene, Cambridge, MA), was added to the eluted protein at a 1:5 ratio (w/w), and 100% cleavage, as assessed using SDS-PAGE, was achieved upon incubating the mixture for 1 h at 37 °C. The mixture was loaded onto a 5-ml bed volume Talon metal affinity resin column (Clontech, Saint-Germain-en-Laye, France); the column was washed with 20 bed volumes of either 20 mM Tris-HCl, pH 7.5, 150 mM KCl, 10 mM imidazole, and 10% glycerol or 40 mM Hepes-OH, pH 7.5, 75 mM KCl, 10 mM imidazole, and 10% glycerol for cross-linking experiments; and HttEx1Qn-His (Fig. 1A) was eluted in the same buffer complemented with 200 mM imidazole. The protein was immediately filtered through a 0.22- μ m filter, aliquoted, flash frozen in liquid nitrogen, and stored at -80 °C until use. The temperature, protein concentration, and buffer conditions were optimized so that the cleaved HttEx1Qn would remain soluble during the whole purification process. HttEx1Qn concentration was determined by SDS-PAGE quantification following SYPRO Orange staining and integration using a LAS-3000 imager (Fujifilm, Tokyo, Japan) and the software Multigauge (Life Science Systems). PolyQ and HttEx1Qn- Δ Nt₁₇ (Fig. 1A) were obtained following the same procedure.

Recombinant His₆-tagged wild type Hsc70, Hdj1, and Hdj2 were purified as described previously (25). Concentrations were determined spectrophotometrically using the following extinction coefficients at 280 nm: 39,310 M⁻¹ cm⁻¹ for Hsc 70, 9970 M⁻¹ cm⁻¹ for Hdj1, and 16,390 M⁻¹ cm⁻¹ for Hdj2. Pure

Hsc70, Hdj1, and Hdj2 in 50 mM Tris-HCl, pH 7.5, 150 mM KCl, 5 mM β -mercaptoethanol, 5 mM MgCl₂, 1 mM EGTA, and 10% glycerol were aliquoted and stored at -80 °C. Hsc70 was also stored in 40 mM Hepes-OH, pH 7.5, 75 mM KCl, 5 mM β -mercaptoethanol, 5 mM MgCl₂, 1 mM EGTA, and 10% glycerol. To ensure that Hsc70 and its co-chaperones were functional, their luciferase refolding activities and their ATPase activities were monitored as described (25).

The peptides Nt₁₇ (MATLEKLMKAFESLKSF), dansyl-Nt₁₇ (Fig. 1A), and its scrambled form (dansyl-MLTFAEFKSMELKSLAK) were purchased from GL Biochem Ltd. (Shanghai, China). Peptides were dissolved in HFIP, aliquoted, and stored after evaporation of HFIP under N₂ at -20 °C. All peptides were resuspended in DMF at a final concentration of 2 mM.

Assembly of HttEx1Qn, PolyQ, or HttEx1Qn- Δ Nt₁₇ into Fibrils and Monitoring of the Aggregation Reactions—Soluble HttEx1Qn, polyQ, and HttEx1Qn- Δ Nt₁₇ were assembled in 20 mM Tris-HCl, pH 7.5, 150 mM KCl, 5 mM MgCl₂, 1 mM ATP, 100 mM imidazole, and 10% glycerol, with or without Hsc70, Hdj1, Hdj2, or Nt₁₇, alone or in combination, at 37 °C without shaking. For thioflavin T measurements, aliquots (100 μ l) were withdrawn and immediately mixed with thioflavin T (10 μ M final). The fluorescence was measured on a Cary Eclipse fluorescence spectrophotometer (Varian Medical Systems Inc., San Diego, CA) using the following settings: excitation wavelength = 440 nm; emission wavelength = 480 nm; excitation and emission slits = 5 and 10 nm, respectively.

For SDS-PAGE analyses, aliquots (8 μ l) were removed at different time intervals, immediately mixed with denaturing buffer (180 mM Tris-HCl, pH 6.8, 30% glycerol, 15% β -mercaptoethanol, 6% SDS), incubated for exactly 5 min at 95 °C, and frozen at -70 °C until analysis on 12–15% glycine-SDS-PAGE. The gels were washed in water, stained by SYPRO Orange (Invitrogen) diluted 5000-fold in acetic acid 10% for 1 h, and visualized using an LAS-3000 imager (Fujifilm, Tokyo, Japan). The amount of SDS-soluble and SDS-insoluble species trapped in the stacking gel was quantified using the software Multigauge (Life Science Systems). For each time point t , the fraction f_t of the assembled polypeptides was extrapolated from these values and plotted *versus* time. The plots were fitted to the following empirical sigmoid function,

$$f_t = f_\infty / (1 + \exp(k_{\text{elong}}(t_{1/2} - t))) \quad (\text{Eq. 1})$$

where f_∞ represents the fraction of assembled polypeptide at the end of the reaction, k_{elong} is the elongation slope, and $t_{1/2}$ is the aggregation half-time. The lag phase duration t_{lag} was determined from k_{elong} and $t_{1/2}$ as follows.

$$t_{\text{lag}} = t_{1/2} - \ln(2/k_{\text{elong}}) \quad (\text{Eq. 2})$$

For each protein variant, we recorded at least three independent kinetics of aggregation. The presence of fibrillar material at the end of the aggregation process was systematically assessed by transmission electron microscopy.

The interaction between Hsc70 and HttEx1Qn was assessed by plotting the inverse of assembly half-times against Hsc70 concentration and fitting the plots to the following exponential function,

Molecular Interaction between Hsc70 and Huntingtin Exon 1

$$1/t_{1/2} = A + (B - A) \cdot \exp(-c_{\text{Hsc70}}/EC_{50}) \quad (\text{Eq. 3})$$

where A is the asymptotic value of $1/t_{1/2}$, B is the value of $1/t_{1/2}$ without Hsc70, c_{Hsc70} is the concentration of Hsc70 in μM , and EC_{50} is the half-maximal effective Hsc70 concentration.

Filter Trap Assay and Western Blotting—The presence of SDS-resistant material formed by HttEx1Q17 and HttEx1Q48 at the end of the aggregation reaction was assessed by a filter retardation assay (26), where 10 μl of each reaction were diluted in triplicate in 200 μl of 2% SDS, filtered through cellulose acetate membrane (0.2- μm pore size, Millipore Corp., Bedford, MA) using a 48-slot slot-blot filtration apparatus (GE Healthcare), and washed twice with 200 μl of 2% SDS. The cellulose acetate membranes were incubated with 3% skim milk, probed with a rabbit polyclonal anti-HttEx1Qn antibody we raised, and developed with the enzyme-coupled luminescence technique (ECL, Thermo Scientific) according to the recommendation of the manufacturer.

Fluorescence Measurements—The binding of dansyl-Nt₁₇ and its scrambled version to Hsc70 or soluble huntingtin-derived polypeptides was determined as follows. Dansyl-Nt₁₇ and its scrambled version (1 μM) were co-incubated alone or with increasing concentrations of Hsc70 and/or HttEx1Q35, HttEx1Q35- ΔNt_{17} , or Gln₃₅ for 10 min at room temperature. The fluorescence of the solution was then recorded on a Cary Eclipse fluorescence spectrophotometer (Varian Medical Systems Inc.) using the following settings: excitation wavelength = 340 nm; emission wavelength = 505 nm; excitation and emission slits = 2.5 and 10 nm, respectively.

Electron Microscopy—Protein assemblies were examined by transmission electron microscopy in a Jeol 1400 transmission electron microscope (Jeol SAS, Croissy-sur-Seine, France) following adsorption onto carbon-coated 200 mesh grids and negative staining with 1% uranyl acetate. The images were recorded with a Gatan Orius CCD camera (Gatan Inc., Pleasanton, CA).

Fourier Transformed Infrared Spectroscopy (FTIR)—HttEx1Q25, HttEx1Q48, and HttEx1Q48 in the presence of equimolar concentrations of Hsc70 were assembled as described above. Fibrillar samples (5 mg) were spun at 16,000 $\times g$ at 25 °C for 20 min and then extensively washed in D₂O. The spectra were recorded on a Jasco FT/IR-600 Plus spectrometer equipped with a nitrogen-cooled MTC detector, using the attenuated total reflectance mode. A total of 512 interferograms were collected at a resolution of 2 cm^{-1} . The sample chamber was continuously purged with CO₂-free air. The background consisted of D₂O and water vapor. All of the spectra were baseline-corrected, smoothed, and normalized prior to further data processing. Because the same small quantity of Hsc70 was found in the pellet when the chaperone was incubated alone or in the presence of aggregating HttEx1Q48, the contribution of Hsc70 was subtracted from the spectra recorded for HttEx1Q48 fibrils formed in the presence of Hsc70.

Spectral analyses were performed using the curve-fitting analysis software of the Spectra Manager package (Jasco). The amide I band (1575–1725 cm^{-1}) of each spectrum was subjected to a fitting procedure using seven Gaussian distributions centered at the frequencies of well characterized secondary structures and lateral chains (27, 28). Each Gaussian was char-

acterized by its frequency and an interval of given width. Each peak width was limited to 25 cm^{-1} , whereas peak heights were left free. The contribution of each curve to the amide I band was assessed by integrating the area under the curve and normalizing to the total area under the amide I band.

Circular Dichroism—For CD measurements, the Nt₁₇ peptide was dissolved in HFIP, aliquoted, stored after evaporation of HFIP under N₂ at –20 °C, and then resuspended at 2 mM in PBS. Far-UV CD spectra were recorded at 20 °C using a JASCO J-810 dichrograph equipped with a thermostated cell holder using a 0.1-cm path length quartz cuvette. Each spectrum was the average of five acquisitions recorded in the 260–195-nm range with 0.5-nm steps, a bandwidth of 1 nm, and a speed of 50 $\text{nm}\cdot\text{min}^{-1}$. The spectra were buffer-corrected.

Cross-linking and Two-dimensional Gel Electrophoresis—HttEx1Q25 (50 μM) in the presence or the absence of Hsc70 (50 μM) was incubated for 1 h at 37 °C in 40 mM Hepes-OH, pH 7.5, 75 mM KCl, 100 mM imidazole, 5 mM MgCl₂, 1 mM ATP, and 10% glycerol. The cross-linking reaction was performed at room temperature for 30 min using BS3-d0/d4 (5 mM), a homobifunctional sulfo-NHS ester cross-linker reagent with an 11.4-Å spacer arm (Pierce). The reaction was terminated by the addition of ammonium bicarbonate (50 mM).

200 μg of cross-linked proteins were resolved by two-dimensional gel electrophoresis using 7-cm pH 4–7 IPG (immobilized pH gradient) strips (Bio-Rad) and the ReadyPrep™ 2-D Starter Kit (Bio-Rad) following the Bio-Rad instruction manual. Briefly, the products of the cross-linking reactions were precipitated in cold acetone, resuspended in the rehydration buffer (Bio-Rad), and loaded onto a 7-cm pH 4–7 ReadyStrip IPG strip (Bio-Rad). The first dimension was performed using the PROTEAN IEF system (Bio-Rad) after active rehydration. For the second dimension, reduced, alkylated, and equilibrated strips were applied on an 8% Tris-glycine SDS-PAGE running gel. Two-dimensional gels were stained with Coomassie Blue.

Peptide Preparation and NanoLC-Linear Ion Trap (LTQ)-Orbitrap Mass Spectrometry Analysis—Cross-linked protein complex spots separated by two-dimensional gel electrophoresis were excised and subjected to tryptic or GluC digestion using the Progest robot, and the digested peptides were extracted as described previously (29). Tryptic peptides were analyzed by nanoLC-LTQ-Orbitrap mass spectrometry analysis, and the nanoLC-MS/MS data were processed as described previously (29), except that the data analysis included lysine, serine, threonine, tyrosine, and the N-terminal amino acid residues as possible cross-linked sites (30) and that the cross-linker was BS3-d0 and BS3-d4. Briefly, nanoLC-MS data were deisotoped using the Decon2LS software (available at the Pacific Northwest National Laboratory Web site). The resulting csv files were further analyzed with viper (available at the Pacific Northwest National Laboratory Web site) (31) to identify, within the nanoLC-MS analysis, the d0/d4 peptide pairs presenting mass differences of 4.0247 Da as a signature of peptides that have reacted with one molecule of BS3-d0/d4. Mass modifications were set to 138.0681 and 142.0928 Da for BS3-d0- and BS3-d4-cross-linked peptides, respectively. A list of peptide pairs with a maximum mass deviation of less than 10 ppm between the experimental mass and the theoretical mass of

each possible cross-linked peptides was generated and used to identify the BS3-d0/d4-cross-linked peptides using their MS/MS spectra and the GPMW (32) and xQuest (33) software. Finally, identification of cross-linked peptides and location of cross-linking sites were manually validated by comparison of the experimental masses and the theoretical masses of the d0/d4 ion fragment pairs calculated for each cross-linked peptide. The peptide pairs listed in Table 2 have a maximum mass deviation of less than 3 ppm.

In Vivo Seeding Assays—We compared the nucleation capacities of HttEx1Q48 fibrils assembled in the absence or the presence of Hsc70 using the assay we established in reporter cell lines (10, 34). In summary, U2OS cells stably expressing soluble mCherry fluorescent protein fused to HttEx1Q25 (HttEx1Q25-ChFP) were grown in McCoy's 5A medium supplemented with 10% FBS, 2 mM glutamine, 100 units/ml penicillin, 100 μ g/ml streptomycin, and 500 μ g/ml G418 on poly-L-lysine-coated coverslips. After 48 h, the cells were treated with 0.5 μ M of HttEx1Q48 fibrils (monomer concentration) assembled in the absence or the presence of equimolar concentrations of Hsc70. After 24 h, the coverslips were washed with PBS, and the amount of HttEx1Q25-ChFP fluorescent foci was determined by direct live measurement of fluorescence and cell counting. Images were acquired on the AxioObserver Z1 epifluorescence microscope equipped with an Incubator chamber XL multi-S1 RED LS (Carl Zeiss) and an Orca-R2 camera (Hamamatsu).

RESULTS

Aggregation of HttEx1Qn of Different PolyQ Lengths—We first established a protocol to purify recombinant soluble HttEx1Qn from the fusion precursor MBP-TEV-HttEx1Qn-His. An additional purification step after cleavage by the MBP-TEV allowed us to recover soluble HttEx1Qn separate from both the carrier protein and the protease. This ensured that the different modifiers of aggregation used throughout this study would not be diverted from HttEx1Qn by the MBP-TEV or the cleaved MBP moiety. We then characterized the aggregation of HttEx1Qn with polyQ stretches ranging from 17 to 48 residues (Fig. 1A). Because HttEx1Qn fibrils bind poorly to thioflavin T, the fluorescent dye commonly used to follow amyloid aggregation, we monitored the kinetics of aggregation not only by thioflavin T binding but also by quantifying SDS-soluble or SDS-insoluble HttEx1Qn species by SDS-PAGE (Fig. 1, B and C). The kinetics of aggregation obtained from these different probes were similar (Fig. 1D).

The kinetics of HttEx1Q17, HttEx1Q25, HttEx1Q30, HttEx1Q35, HttEx1Q41, and HttEx1Q48 (Fig. 1A) aggregation in physiological conditions and at identical concentrations are represented in Fig. 1E. As expected, the longer the polyQ, the faster HttEx1Qn aggregated. Remarkably, we found a highly significant inverse linear correlation between the polyQ length and the logarithm of the aggregation half-time (Fig. 1F; $r^2 = 0.90$; $p = 0.004$). We ascertained that HttEx1Qn of non-pathological polyQ lengths (*i.e.* of less than 35 consecutive Gln) assembled into SDS-resistant fibrils whose conformation was similar to the one adopted by HttEx1Q48 fibrils (Fig. 1G). The amount of fibrillar, SDS-insoluble, material at steady state was

yet variable, with a threshold between 25 and 30 consecutive Gln (Fig. 1H).

Effects of Hsc70 and Its Co-chaperones Hdj1 and Hdj2 on HttEx1Q48 Aggregation—We examined the impact of Hsc70, in its active, functional form, and its co-chaperones on HttEx1Qn aggregation (Figs. 2 and 3). We systematically verified that all chaperones were functional. To this end, we assessed both luciferase refolding and ATP hydrolysis (Figs. 2 (A and B) and 3 (A and B)). Increasing Hsc70 concentrations progressively slowed down the kinetics of HttEx1Q48 aggregation (Fig. 2, C–E). The effect of Hsc70 was even greater in the absence of nucleotides (Fig. 2E). This is consistent with a canonical chaperone functioning. Indeed, in the absence of nucleotide, Hsc70 binds client proteins and does not release them. In the presence of ATP and upon ATP hydrolysis, the Hsc70 client binding site cycles between an open and a closed conformation with simultaneous binding and release of client proteins. The affinity of Hsc70 for soluble HttEx1Q48 in its active, functional form was derived from the corresponding aggregation half-times; the observed EC_{50} was equal to 8 μ M (Fig. 2F). Notably, Hsc70 neither incorporated within the fibrils nor bound preformed fibrils (Fig. 2, G and H).

To add a further level of complexity, we assessed the effect of the Hsc70 co-chaperones Hdj1 and Hdj2, alone or in combination with Hsc70 (Fig. 3). Whereas Hdj2 had a marginal effect on HttEx1Q48 aggregation, Hdj1 significantly affected the reaction (Fig. 3, C–E). Moreover, Hdj1 and Hdj2 acted synergistically with Hsc70 in slowing HttEx1Q48 assembly. In each case, the measured effect of Hdj1 or Hdj2 and Hsc70 was significantly larger than that of the sum of individual chaperones (Fig. 3, E and F).

We then assessed the consequences of Hsc70 presence in HttEx1Q48 aggregation reactions on the resulting assemblies scaffold. HttEx1Q48 assemblies obtained in the presence of equimolar amounts of Hsc70 looked indistinguishable from those formed in the absence of the chaperone in the electron microscope (compare Figs. 4A and 1G (*right*)). To determine whether Hsc70 affects HttEx1Q48 fibrillar architecture, the secondary structure contents of fibrillar HttEx1Q25, HttEx1Q48, and HttEx1Q48 obtained in the presence of equimolar concentrations of Hsc70 were assessed by FTIR spectroscopy. Spectrum deconvolution showed that all of the fibrils contained the amide I bands characteristic of the amyloid structure although to a different extent (Table 1). HttEx1Q25 and HttEx1Q48 fibrils had different secondary structure contents, with HttEx1Q48 being richer in amyloid structure at the expense of non-amyloid β -sheets (Table 1). Remarkably, the FTIR spectra of the HttEx1Q48 fibrils formed in the absence or presence of Hsc70 were markedly different, the latter being more similar to the spectra of HttEx1Q25 fibrils (Fig. 4B and Table 1).

Finally, we assessed the functional properties of HttEx1Q48 fibrils formed in the absence or presence of Hsc70 using the nucleation assay we established in reporter cell lines (U2OS cells) expressing soluble HttEx1Q25-ChFP (10, 34). The endogenous HttEx1Q25-ChFP redistributed into fluorescent foci in 50% of cells exposed to HttEx1Q48 fibrils formed in the absence of Hsc70, whereas only 22% of cells exposed to identical concentrations of HttEx1Q48 fibrils formed in the presence of Hsc70 exhibited puncta (Fig. 4C).

Molecular Interaction between Hsc70 and Huntingtin Exon 1

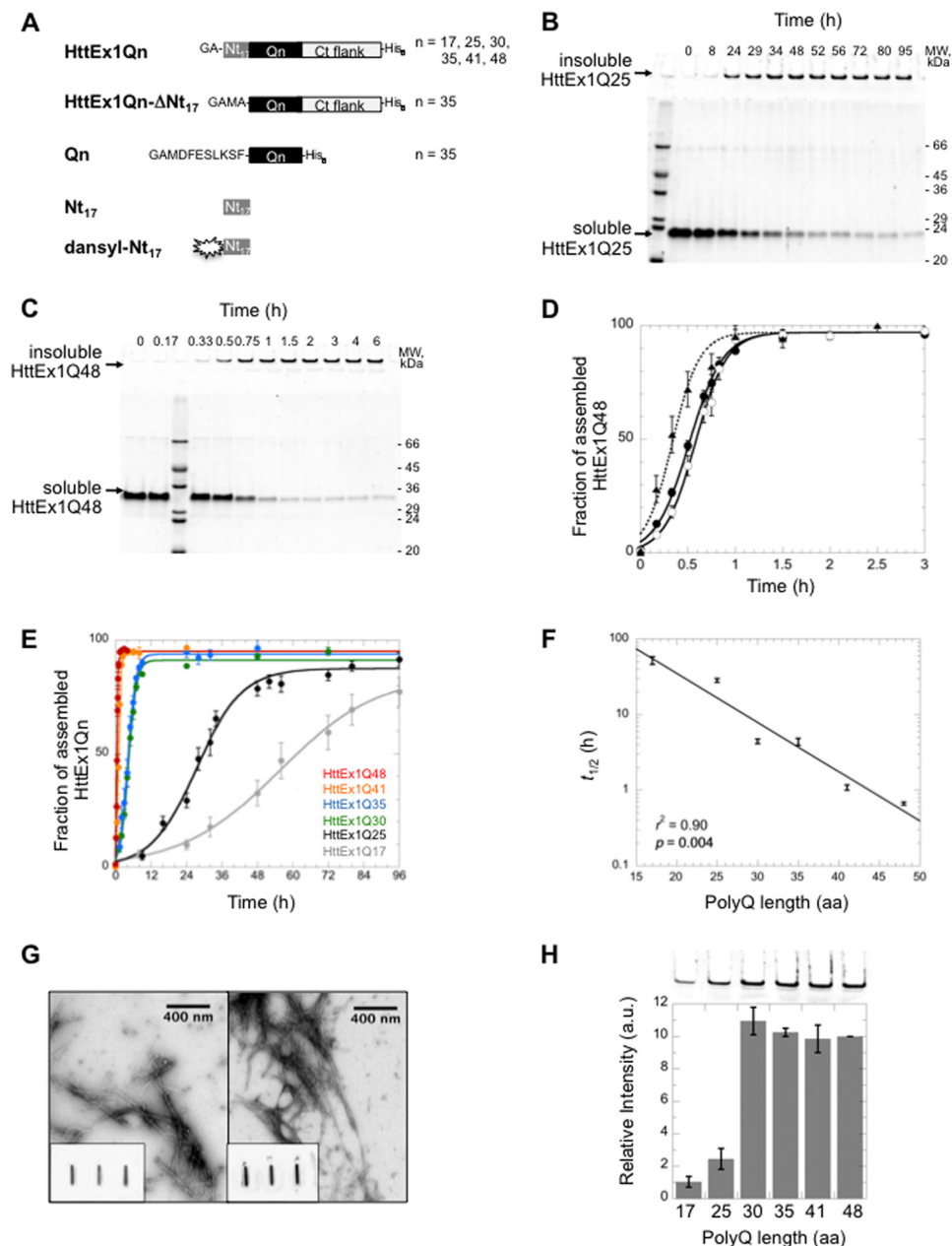


FIGURE 1. Aggregation of HttEx1Qn of pathological and non-pathological lengths. *A*, schematic representation of the primary structure of the different HttEx1Qn-derived polypeptides used in this study. *B* and *C*, monitoring of HttEx1Qn assembly; examples of HttEx1Q25 (*B*) and HttEx1Q48 (*C*) (20 μ M each). For each reaction, aliquots were withdrawn at different time intervals and loaded onto a Tris/glycine SDS-polyacrylamide gel. The gel was then stained with SYPRO Orange, and the bands corresponding to soluble and insoluble HttEx1Qn were quantified. *D*, assembly kinetics of HttEx1Q48 obtained by measuring (i) thioflavin T binding (*triangles*), (ii) the disappearance of SDS-soluble species (*solid circles*), or (iii) the formation of SDS-insoluble aggregates (*open circles*) on SDS-PAGE. In each case, assembly is expressed as a fraction of the maximum signal. Each data point corresponds to the mean and associated S.E. calculated from 3–10 independent experiments. *E*, time course of aggregation for HttEx1Qn (20 μ M) of different polyQ stretch lengths at 37 °C. Each data point corresponds to the mean and associated S.E. calculated from 3–10 independent experiments. *F*, half-time ($t_{1/2}$) of HttEx1Qn aggregation is correlated with the polyQ stretch length. Each data point corresponds to the mean and associated S.E. calculated from 3–10 independent experiments. The *solid line* represents the best linear fit; the r^2 and p values of the linear regression are indicated. *G*, nature of species present at steady state for HttEx1Q17 (*left*) and HttEx1Q48 (*right*), assessed by negative stained electron microscopy and filter trapping in triplicate (*insets*). *H*, SDS resistance of HttEx1Qn fibrils. *Top*, SDS-resistant material present at the end of the aggregation process of HttEx1Qn of different polyQ lengths trapped in the wells of an SDS-PAGE. The gel was stained by SYPRO Orange (Invitrogen), and the signal was quantified using the software Multigauge (Life Science Systems). The relative means and associated S.E. values calculated from three independent experiments are represented at the *bottom*. *a.u.*, arbitrary units.

We conclude from these observations that the interaction of Hsc70 with the soluble forms of HttEx1Qn of pathological length conferred to the latter kinetics, structural, and functional properties characteristic of HttEx1Qn of non-pathological lengths.

Hsc70 Effects on HttEx1Qn Assembly Are Independent of PolyQ Length—Chaperones from the Hsp70 family have been described to interact mostly with solvent-exposed hydrophobic patches on polypeptides (23, 24). Thus, one could wonder how Hsc70 recognizes the main culprit of HttEx1Q48 aggregation

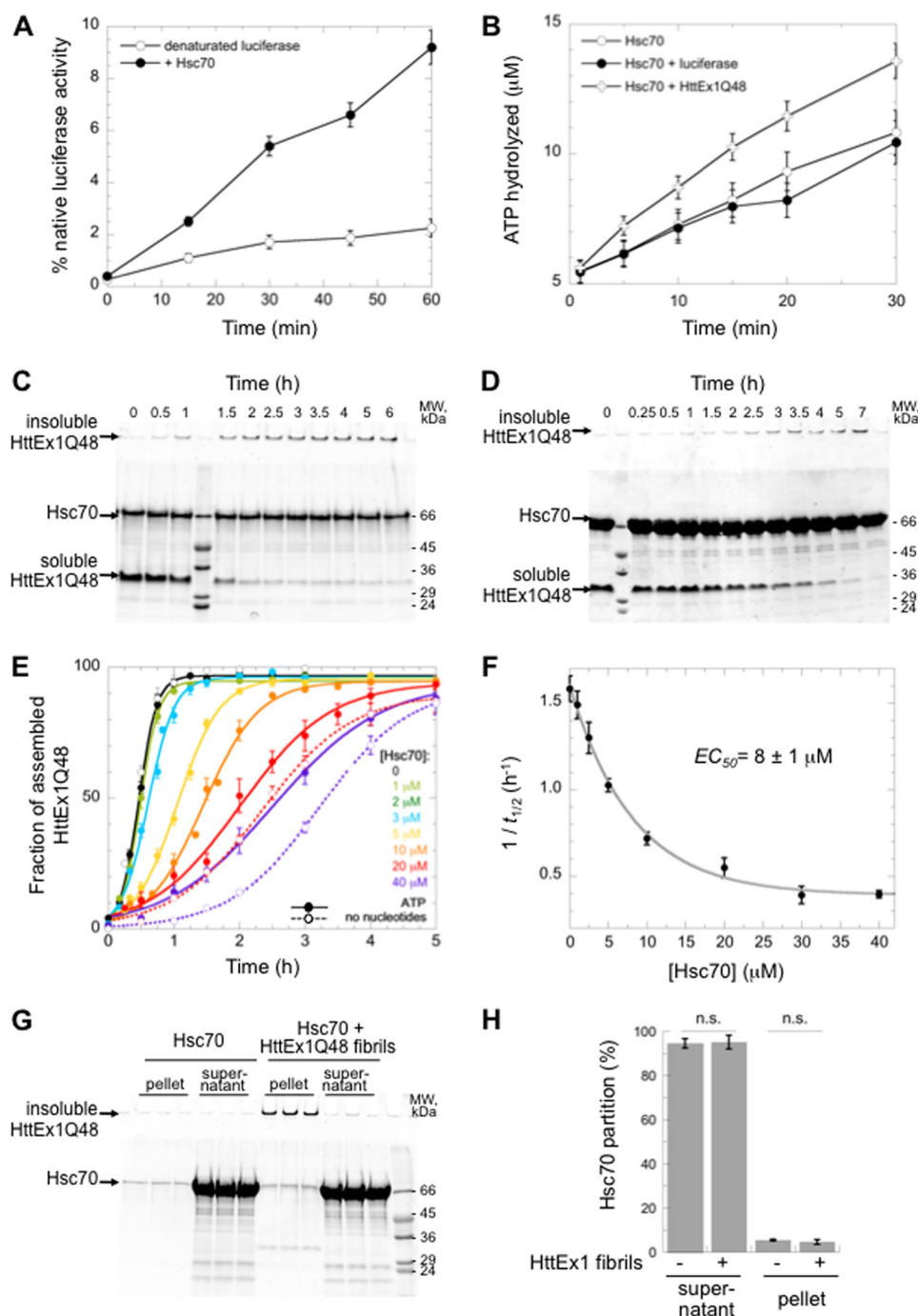


FIGURE 2. Assembly of HttEx1Q48 in the presence of Hsc70. *A* and *B*, activity of Hsc70. *A*, luciferase assay. Refolding of chemically denatured luciferase (0.1 μM) in the absence (open circles) or in the presence of Hsc70 (20 μM ; solid circles). Each data point corresponds to the mean and associated S.E. (error bars) calculated from three independent experiments. *B*, [$\gamma\text{-}^{32}\text{P}$]ATP hydrolysis. Shown is ATPase activity of Hsc70 alone (20 μM ; open circles) and in the presence of luciferase (0.1 μM ; solid circles) or HttEx1Q48 (20 μM ; open crosses). We measured Hsc70 ATPase activity after extraction of the [^{32}P]phosphomolybdate complex formed in 1 N HCl at 30 $^{\circ}\text{C}$ in assembly buffer. Each data point corresponds to the mean and associated S.E. calculated from three independent experiments. *C* and *D*, representative examples of HttEx1Q48 assembly (20 μM) in the presence of 5 μM (*C*) or 20 μM (*D*) Hsc70. For each reaction, aliquots were withdrawn at different time intervals and loaded onto a Tris/glycine SDS-polyacrylamide gel. The gel was then stained with SYPRO Orange, and the bands corresponding to soluble and insoluble HttEx1Q48 were quantified. *E* and *F*, effect of Hsc70 on HttEx1Q48 kinetics of assembly. *E*, time courses of HttEx1Q48 (20 μM) assembly at 37 $^{\circ}\text{C}$ with increasing concentrations of Hsc70 (0–40 μM) in the absence (dashed lines) or the presence (solid lines) of 1 mM ATP. Each data point corresponds to the mean and associated S.E. calculated from 3–10 independent experiments. *F*, half-maximal effective Hsc70 concentration. The inverse of assembly half-time ($1/t_{1/2}$) for HttEx1Q48 at a constant concentration (20 μM) was determined for increasing Hsc70 concentrations (0–40 μM). Each data point corresponds to the mean and associated S.E. calculated from 3–10 independent experiments. *G* and *H*, Hsc70 does not bind to HttEx1Qn fibrils. Hsc70 (20 μM) was incubated alone or in the presence of HttEx1Q48 fibrils (20 μM monomer concentration) for 1 h at 37 $^{\circ}\text{C}$. The reaction was done in triplicate. The reaction mixtures were centrifuged for 20 min at 16,000 $\times g$, and the corresponding pellets and supernatants were loaded onto an SDS-polyacrylamide gel (*G*). The gel was then stained with SYPRO Orange, the bands corresponding to Hsc70 in the pellet and the supernatant were quantified, and the calculated mean and S.E. values are represented (*H*). Statistical significance corresponds to Student's *t* tests. *n.s.*, not significant.

Molecular Interaction between Hsc70 and Huntingtin Exon 1

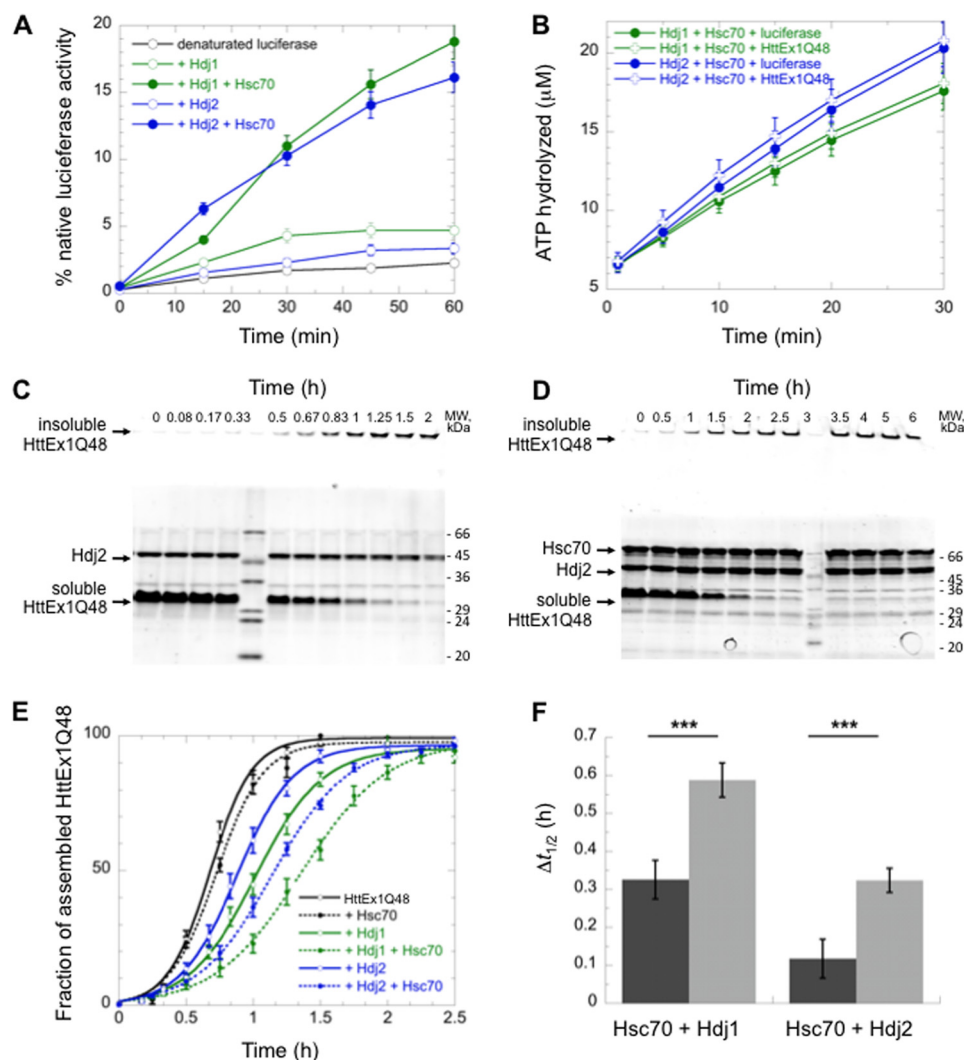


FIGURE 3. Assembly of HttEx1Q48 in the presence of the co-chaperones Hdj1 and Hdj2. *A* and *B*, activity of the co-chaperones. *A*, luciferase assay. Refolding of chemically denatured luciferase (0.1 μM) in the absence (*open circles*) or in the presence of Hdj1 or Hdj2 (20 μM each; *solid circles*). Each data point corresponds to the mean and associated S.E. (*error bars*) calculated from three independent experiments. *B*, [γ - ^{32}P]ATP hydrolysis. Shown is ATPase activity of Hdj1 and Hsc70 (*green*; 10 μM each) or Hdj2 and Hsc70 (*blue*; 10 μM each) in the presence of luciferase (0.1 μM ; *solid circles*) or HttEx1Q48 (20 μM ; *open crosses*). Each data point corresponds to the mean and associated S.E. calculated from three independent experiments. *C* and *D*, representative examples of HttEx1Q48 assembly (20 μM) in the presence of Hdj2 (2.5 μM) and in the absence (*C*) or the presence (*D*) of Hsc70 (2.5 μM). For each reaction, aliquots were withdrawn at different time intervals and loaded onto a Tris/glycine SDS-polyacrylamide gel. The gel was then stained with SYPRO Orange, and the bands corresponding to soluble and insoluble HttEx1Q48 were quantified. *E*, time courses of HttEx1Q48 (20 μM) assembly at 37 $^{\circ}\text{C}$ in the absence or presence of Hsc70 and/or Hdj1 or Hdj2 (2.5 μM each). Each data point corresponds to the mean and associated S.E. calculated from three independent experiments. *F*, effect of the presence of both Hsc70 (2.5 μM) and one co-chaperone (Hdj1 or Hdj2; 2.5 μM each) on HttEx1Q48 assembly half-time at 20 μM . *Black*, calculated theoretical additive effects of the individual chaperones; *gray*, experimental measurements. Each data point corresponds to the mean and associated S.E. calculated from three independent experiments. Statistical significance corresponds to Student's *t* tests; ***, $p < 0.001$.

(i.e. the highly polar expanded polyglutamine stretch). To determine whether Hsc70 interacts with the HttEx1Qn polyglutamine stretch, the kinetics of aggregation of HttEx1Q41, HttEx1Q35, HttEx1Q30, HttEx1Q25, and HttEx1Q17 with increasing concentrations of Hsc70 were monitored as for HttEx1Q48. Similarly to what we observed for HttEx1Q48, Hsc70 slowed down the aggregation of all of the HttEx1Qn we tested (Fig. 5, *A–E*). Hsc70 also reduced the quantity of SDS-insoluble species formed at steady state (Fig. 5, *A–E*). We derived from the assembly kinetics the EC_{50} of the Hsc70-HttEx1Qn interactions. All of the measured EC_{50} values were between 2 and 6 μM (Fig. 5, *F–J*) (i.e. in the range of the Hsc70-HttEx1Q48 interaction) (Fig. 2*F*). The differences we observed were within the experimental errors and did not depend on

polyQ stretch length. We conclude from these measurements that Hsc70 slows down the aggregation of HttEx1Qn in a polyQ length-independent manner.

Hsc70 Interacts with the N-terminal Flank of HttEx1Qn—The fact that Hsc70 interacts to a similar extent with HttEx1Qn displaying polyQ stretches ranging from 17 to 48 Gln residues suggests that it recognizes the polyQ-adjacent flanks (e.g. either the Nt_{17} or the Pro-rich, 53-residue-long C-terminal portion of HttEx1Qn). We first focused on Nt_{17} because it influences the *in vivo* aggregation of the huntingtin protein in many different ways (35–38) and is proposed to initiate the aggregation of HttEx1Qn *in vitro* (see Ref. 39 for a review). To determine whether Hsc70 could interact with HttEx1Qn through Nt_{17} , we compared the aggregation of HttEx1Q35- ΔNt_{17} and Gln₃₅ (Fig.

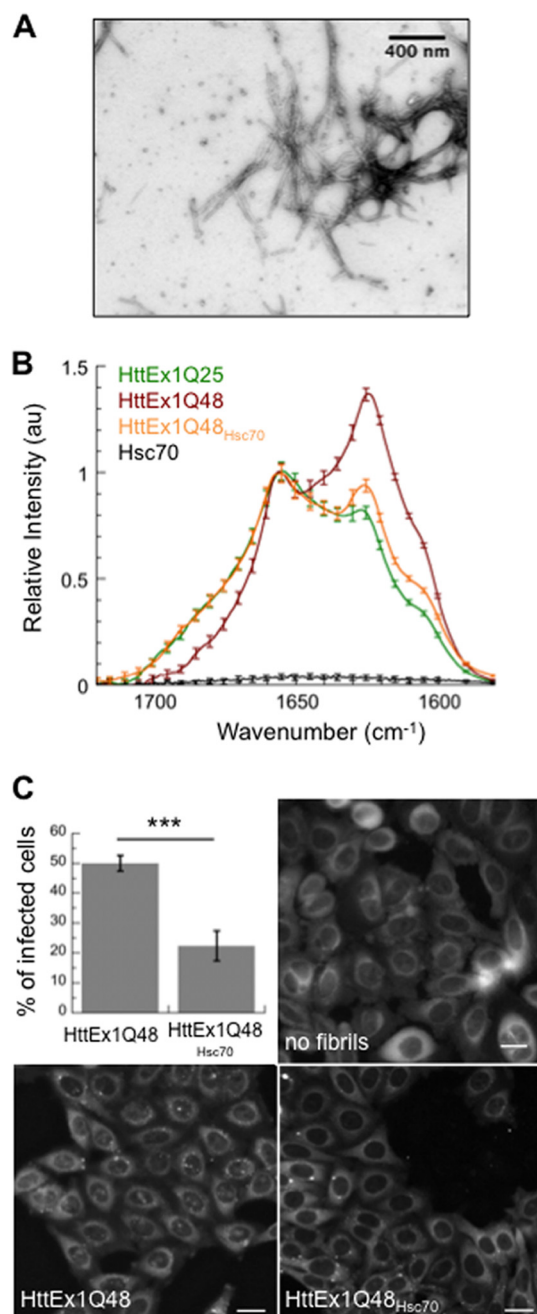


FIGURE 4. Structure-function relationship for HttEx1Q48 fibrils assembled in the absence or the presence of Hsc70. *A*, negative stained electron micrographs of HttEx1Q48 (20 μM) assembled in the presence of Hsc70 at equimolar concentration. *B*, FTIR spectra of fibrillar HttEx1Q25 (green), HttEx1Q48 (red), and HttEx1Q48 assembled in the presence of equimolar concentrations of Hsc70 (HttEx1Q48_{Hsc70}; orange). Because the same small quantity of Hsc70 was found in the pellet when the chaperone was incubated alone or in the presence of aggregating HttEx1Q48, the HttEx1Q48_{Hsc70} spectrum is shown without the contribution of Hsc70; the latter is shown in black. Each data point corresponds to the mean calculated from three independent experiments; for the sake of clarity S.E. values (error bars) are shown every 5 cm^{-1} . *a.u.*, absorbance units. The secondary structure contents are given in Table 1. *C*, nucleation propensities of HttEx1Q48 and HttEx1Q48_{Hsc70} fibrils. The percentage of U2OS cells stably expressing the reporter protein HttEx1Q25-ChFP, with at least one focal HttEx1Q25-ChFP after treatment with exogenous HttEx1Q48 and HttEx1Q48_{Hsc70} fibrils (0.5 μM monomer concentration), is indicated. Each data point corresponds to the mean and associated S.E. calculated from four independent experiments. Statistical significance corresponds to Student's *t* tests; ***, $p < 0.001$. Representative fluorescence micrographs of U2OS cells stably expressing the reporter protein HttEx1Q25-ChFP exposed or not to HttEx1Q48 and HttEx1Q48_{Hsc70} fibrils are shown. Scale bar, 20 μm .

TABLE 1

Secondary structure content of different types of HttEx1Qn fibrils estimated from FTIR spectroscopy measurements

Secondary structure	HttEx1Q25 fibrils	HttEx1Q48 fibrils	HttEx1Q48 fibrils formed in the presence of Hsc70
	%	%	%
Lateral chains	9	13	13
Amyloid	28	43	30
β -Sheets (non-amyloid)	16	3	14
α -Helices	13	12	12
Others	34	31	29

1A) in the absence and the presence of Hsc70. In contrast to what was observed for HttEx1Qn, Hsc70 had no effect on the kinetics of aggregation of HttEx1Q35- ΔNt_{17} or Gln₃₅ (Fig. 6, *A* and *B*).

To further demonstrate that Hsc70 interacts indeed with Nt₁₇, the effect of Hsc70 on HttEx1Q48 aggregation in the presence or the absence of free Nt₁₇ was compared (Fig. 6*C*). As reported previously (40, 41), free Nt₁₇ slowed down the aggregation of HttEx1Q48. The observed inhibitory effect was lifted when Nt₁₇ was preincubated with Hsc70 prior to the addition to HttEx1Q48 (Fig. 6, *C* and *D*). Thus, Hsc70 and Nt₁₇ had antagonistic effects on HttEx1Q48 aggregation, suggesting that Hsc70 sequesters Nt₁₇, thus reducing its free concentration in solution. We next assessed Nt₁₇ interaction with Hsc70 using a fluorescent Nt₁₇ peptide. The specific fluorescence of N-terminally dansyl-labeled Nt₁₇ (Fig. 1*A*) increased upon the addition of increasing concentrations of Hsc70 (Fig. 6*E*). The increased fluorescence intensity indicated that Nt₁₇ peptide was in a more hydrophobic environment following its interaction with Hsc70. A scrambled version of dansyl-Nt₁₇ interacted to a lesser extent with Hsc70, and free dansyl did not interact at all (Fig. 6*E*). The fact that scrambled dansyl-Nt₁₇ still binds to Hsc70, although to a lesser extent than normal dansyl-Nt₁₇, is certainly due to the ability of Hsc70 to bind to most peptides composed of non-polar amino acids and limited selectivity (23). Finally, we saw a competition between Hsc70 and HttEx1Q35 for dansyl-Nt₁₇ binding (Fig. 6*E*), in agreement with the competition between Hsc70 and Nt₁₇ for HttEx1Q35 reported in Fig. 6*C*. These results suggest that Hsc70 binds Nt₁₇ within HttEx1Qn.

We next mapped the surface interfaces between Hsc70 and HttEx1Qn using chemical cross-linking with the homobifunctional NHS-ester BS3 cross-linker and mass spectrometry, using a strategy that we developed previously to assess Hsc70 interaction with another client protein and described in detail previously (29). Hsc70 interacts in a similar way with all of the soluble forms of HttEx1Qn we tested (Fig. 5). We therefore used HttEx1Q25 in the cross-linking studies because, despite being able to assemble into fibrils, it remains soluble for a sufficient time in solution to allow cross-linking (see Fig. 1*E*). Hsc70 and HttEx1Q25 were first allowed to interact for 1 h at 37 $^{\circ}\text{C}$, and the complexes were cross-linked with a mixture of non-deuterated (d0) and deuterated (d4) NHS-ester BS3. The resulting complexes were resolved by two-dimensional gel electrophoresis (Fig. 7*A*) and trypsin-digested in the gel, and the identity of the resulting peptides was determined by nanoLC-MS/MS LTQ-Or-

Molecular Interaction between Hsc70 and Huntingtin Exon 1

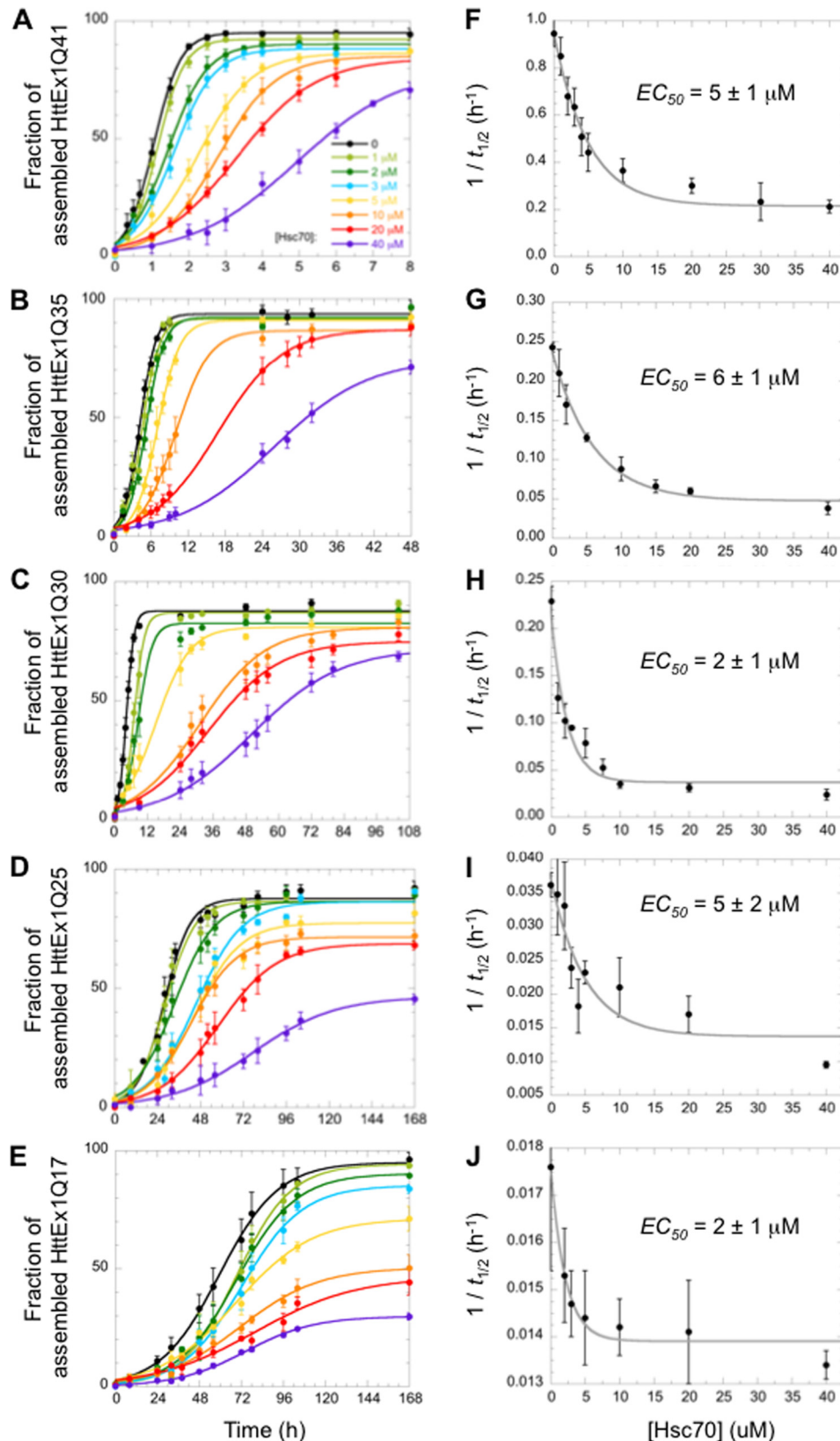


FIGURE 5. Hsc70 affects the assembly of HttEx1Qn of pathological and non-pathological lengths to a similar extent. Left, time courses of HttEx1Qn (20 μM) assembly at 37 $^{\circ}\text{C}$ with increasing concentrations of Hsc70 (0–40 μM). Right, half-maximal effective Hsc70 concentrations. The inverses of assembly half-times ($1/t_{1/2}$) for HttEx1Qn at a constant concentration (20 μM) were determined for increasing Hsc70 concentrations (0–40 μM). A and F, HttEx1Q41; B and G, HttEx1Q35; C and H, HttEx1Q30; D and I, HttEx1Q25; E and J, HttEx1Q17. Each data point corresponds to the mean and associated S.E. values (error bars) calculated from 3–6 independent experiments.

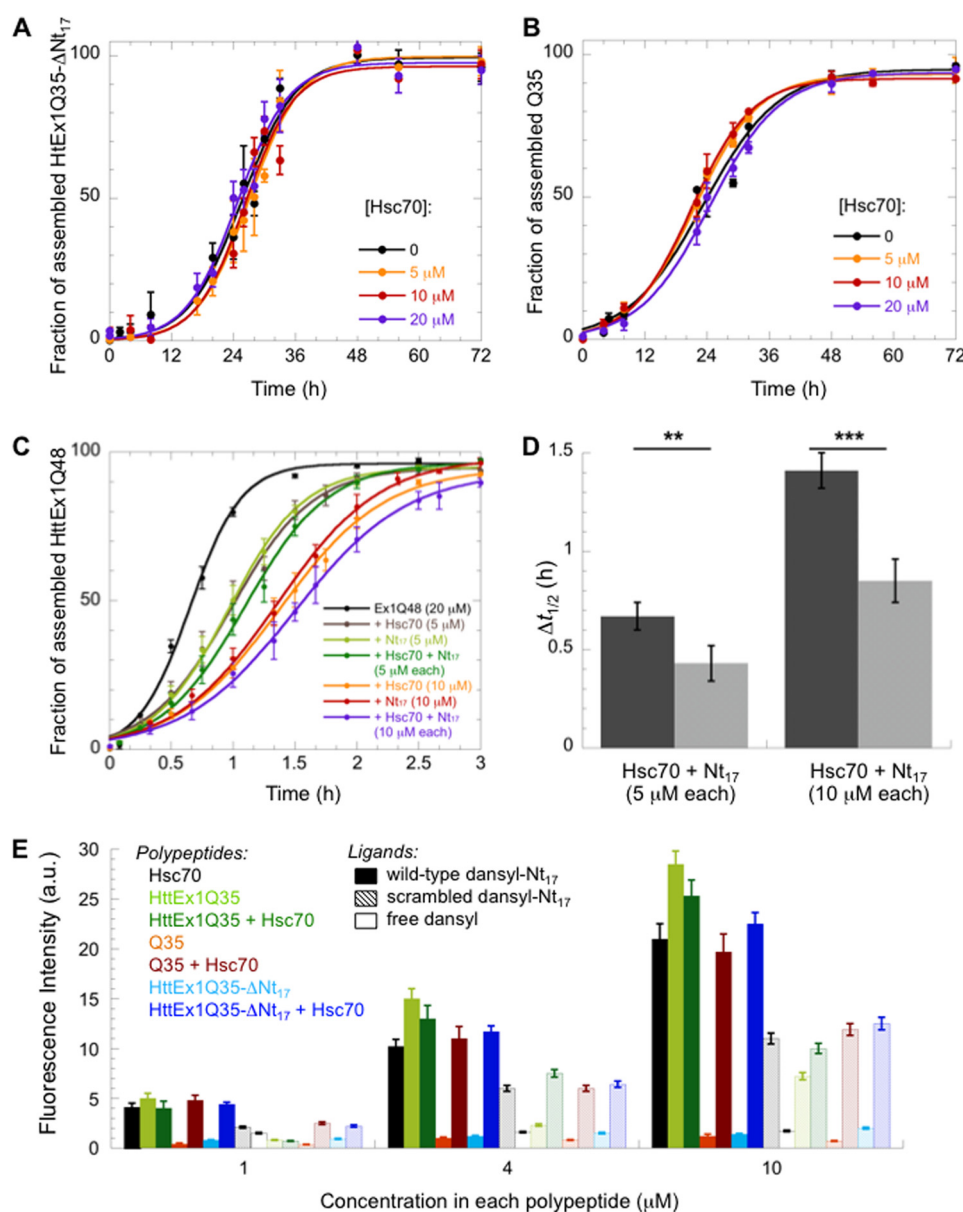


FIGURE 6. Hsc70 interacts with the 17 N-terminal amino acid residues of HttEx1Qn. *A* and *B*, Hsc70 has no effect on HttEx1Qn-ΔNt₁₇ and polyQ assembly. Shown are time courses of HttEx1Q35-ΔNt₁₇ (*A*) and Gln₃₅ (*B*) (20 μM each) assembly at 37 °C with increasing concentrations of Hsc70 (0–20 μM). Each data point corresponds to the mean and associated S.E. values (error bars) calculated from three independent experiments. *C* and *D*, antagonistic effects of Hsc70 and free Nt₁₇ on HttEx1Q48 (20 μM) assembly at 37 °C in the absence or presence of Hsc70 with or without Nt₁₇ at the indicated concentrations. *D*, effect of the presence of both Hsc70 and Nt₁₇ at the indicated concentrations on HttEx1Q48 (20 μM) assembly half-times (Δt_{1/2}). Black, theoretical additive effects of the individual polypeptides; gray, experimental measurements. Each data point corresponds to the mean and associated S.E. calculated from three independent experiments. Statistical significances correspond to Student's *t* tests: ***, *p* < 0.001; **, *p* < 0.01. *E*, binding of dansyl-Nt₁₇ (1 μM; solid columns) to increasing concentrations of Hsc70, HttEx1Q35, Gln₃₅, or HttEx1Q35-ΔNt₁₇, alone or in combination. As controls, we also tested the binding of a scrambled version of dansyl-Nt₁₇ (1 μM; dashed columns) and of free dansyl (1 μM; empty column). Each data point corresponds to the mean and associated S.E. calculated from 3–6 independent experiments. a.u., arbitrary units.

bitrap and both MS and MS/MS data analysis, as described under “Experimental Procedures” and in Ref. 29. Seven Hsc70-HttEx1Q25 cross-links were identified (Table 2). Hsc70 lysine residues involved in the interaction with HttEx1Q25 are mapped on the three-dimensional model of the Hsc70 client polypeptide binding site we built (29). The identification of two representative cross-links is illustrated in Fig. 7, *C–H*. The MS spectra of the triple-charged Hsc70(494–500)-HttEx1Q25(1–8) and triple-charged Hsc70(551–561)-HttEx1Q25(9–17) cross-links with *m/z* 579.6293/580.9713 and 813.1016/814.4431 ion pairs for the BS3-d0 and BS3-d4 peptides are presented in Fig. 7 (*C* and *F*,

respectively). The LTQ-Orbitrap fragmentation mass spectra of the BS3-d4 ions with *m/z* 580.97 and BS3-d0 with *m/z* 813.4362 are shown in Fig. 7 (*D* and *G*, respectively). Finally, the Hsc70 and HttEx1Q25 sequences of the cross-linked peptides identified through *y* and *b* fragment ions are displayed in Fig. 7 (*E* and *H*). The complete list of identified cross-links involving Hsc70 residues 452–469, 494–500, 551–561, 558–567, and 558–569 and HttEx1Q25(1–8) and HttEx1Q25(9–17) is given in Table 2. All of the cross-linked lysine residues identified within Hsc70 (Lys-458, -497, -557, and -561) are situated within its client protein binding domain. All of the cross-linked residues identified within

Molecular Interaction between Hsc70 and Huntingtin Exon 1

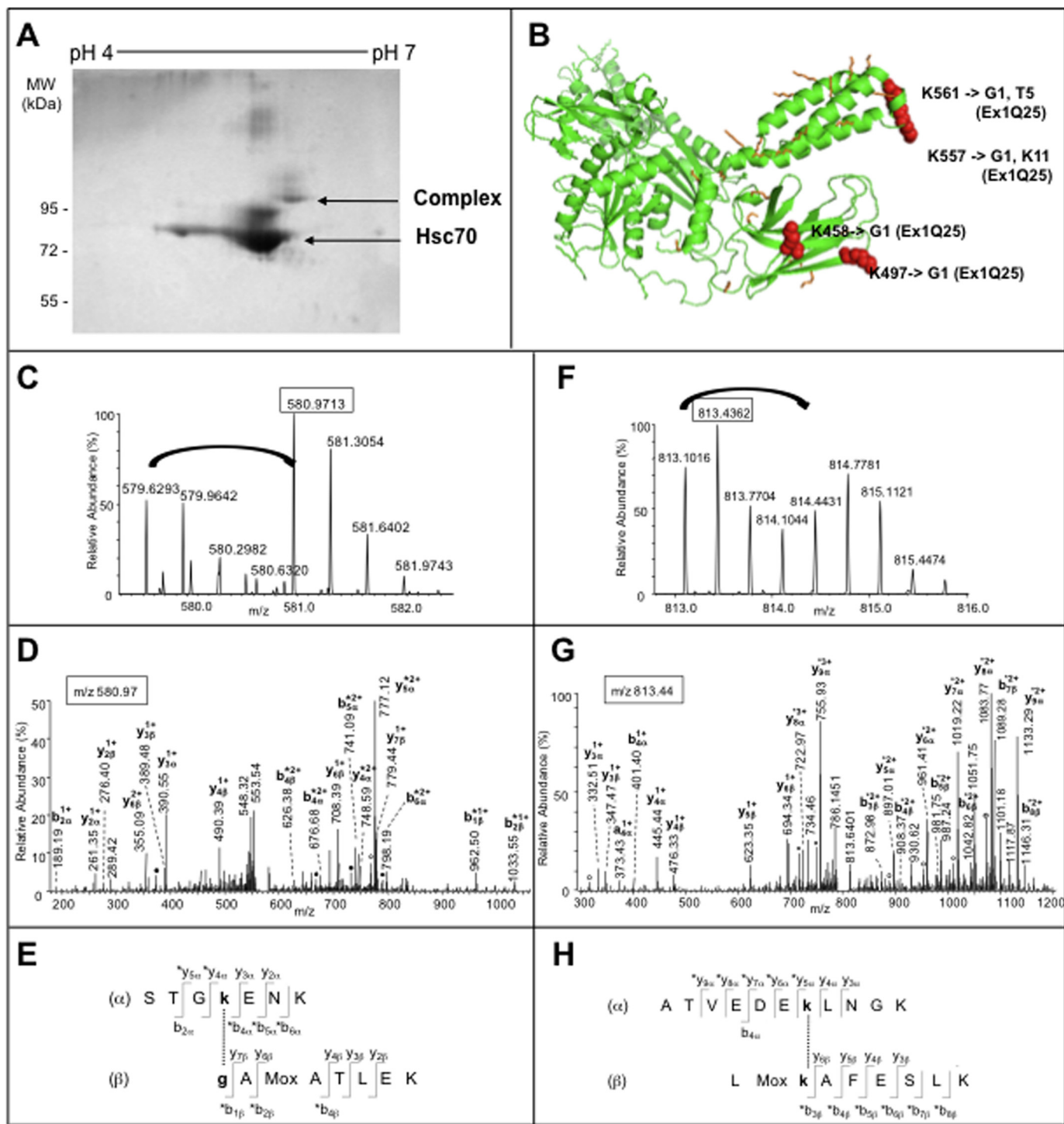


FIGURE 7. Identification of HttEx1Q25-Hsc70 interaction sites. *A*, Coomassie Blue-stained two-dimensional gel of the reaction products generated upon Hsc70 and HttEx1Q25 cross-linking using BS3-d0/d4. *B*, location of the Hsc70 lysine residues cross-linked to HttEx1Q25. The cross-linked peptides are given in Table 2. Lysine residues are depicted as orange sticks, and cross-linked lysines are colored in red and shown as atom spheres. For each lysine from Hsc70 cross-linked to HttEx1Q25, the cross-linked threonine, lysine, or N-terminal glycine residue from HttEx1Q25 is indicated. The Hsc70 three-dimensional model was built as described by Redeker *et al.* (29). This figure was generated using PyMOL (Schroedinger, LLC, New York). *C–E*, identification of the cross-link between peptide 494–500 from Hsc70 and peptide 1–8 from HttEx1Q25. *C*, mass spectrum of the triple-charged cross-linked peptide with monoisotopic m/z 579.6293 and 580.9713 for the BS3-d0 and BS3-d4 peptides, respectively. *D*, fragmentation spectrum of the precursor ion at m/z 580.97, corresponding to the first isotope of the BS3-d4 peptide. The identified fragments and their charge state are annotated. The asterisks indicate the fragments with the BS3-d4 cross-linker. *E*, the identified fragments are indicated on the cross-linked sequences. The α and β sequences correspond to the Hsc70(494–500) and HttEx1Q25(1–8) peptides, respectively. This cross-link involves residues Lys-497 and the N-terminal Gly-1 from Hsc70 and HttEx1Q25, respectively. *F–H*, identification of the cross-link between peptides Hsc70(551–561) and HttEx1Q25(9–17). *F*, mass spectrum of the triple-charged cross-linked peptide with monoisotopic m/z 813.1016 and 814.4431 for the BS3-d0 and BS3-d4 peptides, respectively. *G*, fragmentation spectrum of the precursor ion at m/z 813.4362, corresponding to the second isotope of the BS3-d0 peptide. The identified fragments are annotated, together with their charge state. The asterisks indicate the fragments with the BS3-d0 cross-linker. *H*, the identified fragments are indicated on the cross-linked sequences. The α and β sequences correspond to the Hsc70(551–561) and HttEx1Q25(9–17) peptides, respectively. This cross-link involves residues Lys-557 and Lys-11 from Hsc70 and HttEx1Q25, respectively.

TABLE 2

List of the identified Hsc70-HttEx1Q25 cross-linked peptides

For each identified cross-linked peptide in the Hsc70-HttEx1Q25 complex, the table gives the experimental mass (M_{exp}), the charge state (z), the m/z ratio for both the BS3G-d0- and the BS3-d4-cross-linked peptides, the amino acid segment, the cross-linked residues (XL site) in lowercase boldface type, and the amino acid sequence for both the Hsc70 and the HttEx1Q25 peptides. ΔM (ppm) corresponds to the mass deviation between the experimental mass and the theoretical mass of the identified BS3-d0-cross-linked peptides, given by the XBobCat software (available on the ETH Web site) (33). M(Ox), oxidized methionine.

BS3-d0 peptides			BS3-d4 peptides			Hsc70 peptides			HttEx1Q25 peptides			ΔM
M_{exp}	z	m/z	M_{exp}	z	m/z	Segment	XL site	Sequence	Segment	XL site	Sequence	
1735.8644	3	579.63	1739.89043	3	580.97	494–500	Lys-497	STGkENK	1–8	Gly-1	gAM(Ox)ATLEK	1.8
2132.0678	3	711.70	2136.09353	3	713.04	558–567	Lys-561	LQGkINDEDK	1–8	Gly-1	gAM(Ox)ATLEK	2.6
2190.1100	3	731.05	2194.13273	3	732.39	551–561	Lys-557	ATVEDEkLQgK	1–8	Gly-1	gAM(Ox)ATLEK	2.7
2388.2199	4	598.06	2388.2415	4	598.07	558–569	Lys-561	LQGkINDEDKQK	1–8	Gly-1, Thr-5	gAM(Ox)ATLEK	1.7
2436.2813	3	813.10	2440.30583	3	814.44	551–561	Lys-557	ATVEDEkLQgK	9–17	Lys-11	LM(Ox)kAFESLK	1.7
2924.5319	3	975.85	2928.52043	3	977.18	452–469	Lys-458	DNNLLGkFELTGIPPAPR	1–8	Gly-1	gAM(Ox)ATLEK	1.7
3160.5823	4	791.15	3164.6023	4	792.16	551–569	Lys-561	ATVEDEkLQGkINDEDKQK	1–8	Gly-1	gAM(Ox)ATLEK	2

HttEx1Q25 (Gly-1, Thr-5, and Lys-11) are in HttEx1Q25 Nt₁₇. Thus, Hsc70 unequivocally binds HttEx1Qn through the polypeptide that flanks N-terminally the polyQ stretch.

Hsc70 Binding to the N-terminal Flank of HttEx1Qn Shields a Sequence Essential for the Aggregation Process—The HttEx1Qn N-terminal flank has been reported to impact aggregation *in vitro*, possibly through the establishment of homotypic Nt₁₇-Nt₁₇ interactions that would allow the coalescence of the HttEx1Qn molecules (39). Free Nt₁₇ yields CD spectra typical of coiled-coil structures in solution (Fig. 9A). To assess the existence of Nt₁₇-Nt₁₇ interactions within aggregating HttEx1Qn, HttEx1Q25 was allowed to oligomerize for 1 h at 37 °C. The oligomers were cross-linked with a mixture of non-deuterated (d0) and deuterated (d4) NHS-ester BS3, resolved by SDS-PAGE, and trypsin-digested in the gel, and the identity of the resulting peptides was determined by nanoLC-MS/MS LTQ-Orbitrap analyses (29).

A single intermolecular cross-link was identified, as illustrated in Fig. 8 (A–C). The MS spectrum of the triple-charged HttEx1Q25-HttEx1Q25 cross-links with m/z 905.4527/907.4648 ion pairs for the BS3-d0 and BS3-d4 peptides is shown in Fig. 8A. The LTQ-Orbitrap fragmentation mass spectra of the BS3-d0 and BS3-d4 ions are shown in Fig. 8B (*top* and *bottom spectra*, respectively). Finally, the HttEx1Q25(1–8)-HttEx1Q25(1–8) sequence of the cross-linked peptide identified through y and b fragment ions is presented in Fig. 8C. HttEx1Q25 is cross-linked to another HttEx1Q25 through the N-terminal residue of its N-terminal flank. These results show unequivocally that HttEx1Qn molecules interact during fibril formation through their moiety that flanks N-terminally the polyQ stretch.

Finally, we assessed the specific contribution of these Nt₁₇-Nt₁₇ interactions to the aggregation process. HttEx1Q35 aggregates faster than variants of similar polyQ length devoid of Nt₁₇ (Q35 or HttEx1Q35- Δ Nt₁₇), suggesting that the Nt₁₇ contributes to the aggregation process of HttEx1Qn (Fig. 8D). To demonstrate that this is indeed the case, we monitored the aggregation of HttEx1Q35, Gln₃₅, and HttEx1Q35- Δ Nt₁₇ with increasing concentration of free Nt₁₇ added to compete with the N-terminal flank when present. Although free Nt₁₇ slowed down the aggregation of HttEx1Q35 (Fig. 8E), it impacted neither HttEx1Q35- Δ Nt₁₇ (Fig. 8F) nor Gln₃₅ (Fig. 8G) aggregation. Further demonstration of direct interaction between Nt₁₇ and HttEx1Q35 came from the increase of fluorescence intensity upon incubation of dansyl-Nt₁₇ with HttEx1Q35, whereas

no such increase was observed upon incubation with HttEx1Q35- Δ Nt₁₇ or Gln₃₅ (Fig. 6E). Altogether, these observations demonstrate that free Nt₁₇ binds to HttEx1Q35 and interfere in a competitive manner with the initial step of HttEx1Q35 fibrils formation. We conclude from our observations that HttEx1Qn N-terminal flanks drive the coalescence of the molecules during the early stages of assembly.

DISCUSSION

Molecular chaperones are the first line of defense against the aggregation of the cellular proteins involved in neurodegenerative diseases. The guardian activity of chaperones is based on their ability to bind stretches of aggregation-prone hydrophobic residues that are exposed to the solvent in unstructured or misfolded proteins (23, 24). An intriguing question in this respect was whether or not the alleviating effect of Hsc70 on the toxicity of the polyQ-expanded huntingtin protein observed *in vivo* (15, 17, 18, 42, 43) reflected a presumably unfavorable direct interaction between the chaperone and the aggregation-prone polyQ stretch.

Here we define the molecular mechanism by which human Hsc70 interferes with the aggregation of recombinant HttEx1Qn. We show that Hsc70 binds directly to soluble but not fibrillar HttEx1Qn and that the interaction of soluble HttEx1Qn with Hsc70 affects not only the assembly kinetics into fibrils but also the fibrillar scaffold and its functional properties. We next unequivocally demonstrate that Hsc70 binds to a sequence adjacent to the polyQ stretch and map this interaction at the residue level. Finally, we elucidate the primary role of this sequence in the aggregation of HttEx1Qn, thus clarifying both the modes of Hsc70 action and the coalescence of HttEx1Qn molecules prior to their assembly into fibrils.

Aggregation of HttEx1Qn of Pathological and Non-pathological PolyQ Lengths; the Threshold Issue—We first characterized the aggregation of HttEx1Qn of pathological ($n = 48, 41, \text{ or } 35$) and non-pathological lengths ($n = 30, 25, \text{ or } 17$). For the first time to our knowledge, HttEx1Qn of non-pathological polyQ lengths is shown to form fibrils presenting amyloid-like characteristics. The aggregation of HttEx1Qn with short and long polyQ stretches only differed by its assembly kinetics. The lag phases preceding assembly and the elongation slopes varied with the polyQ stretch length. The shorter the polyQ stretch, the longer was the nucleation phase and the lower was the elongation slope. As reported previously for naked synthetic polyQ

Molecular Interaction between Hsc70 and Huntingtin Exon 1

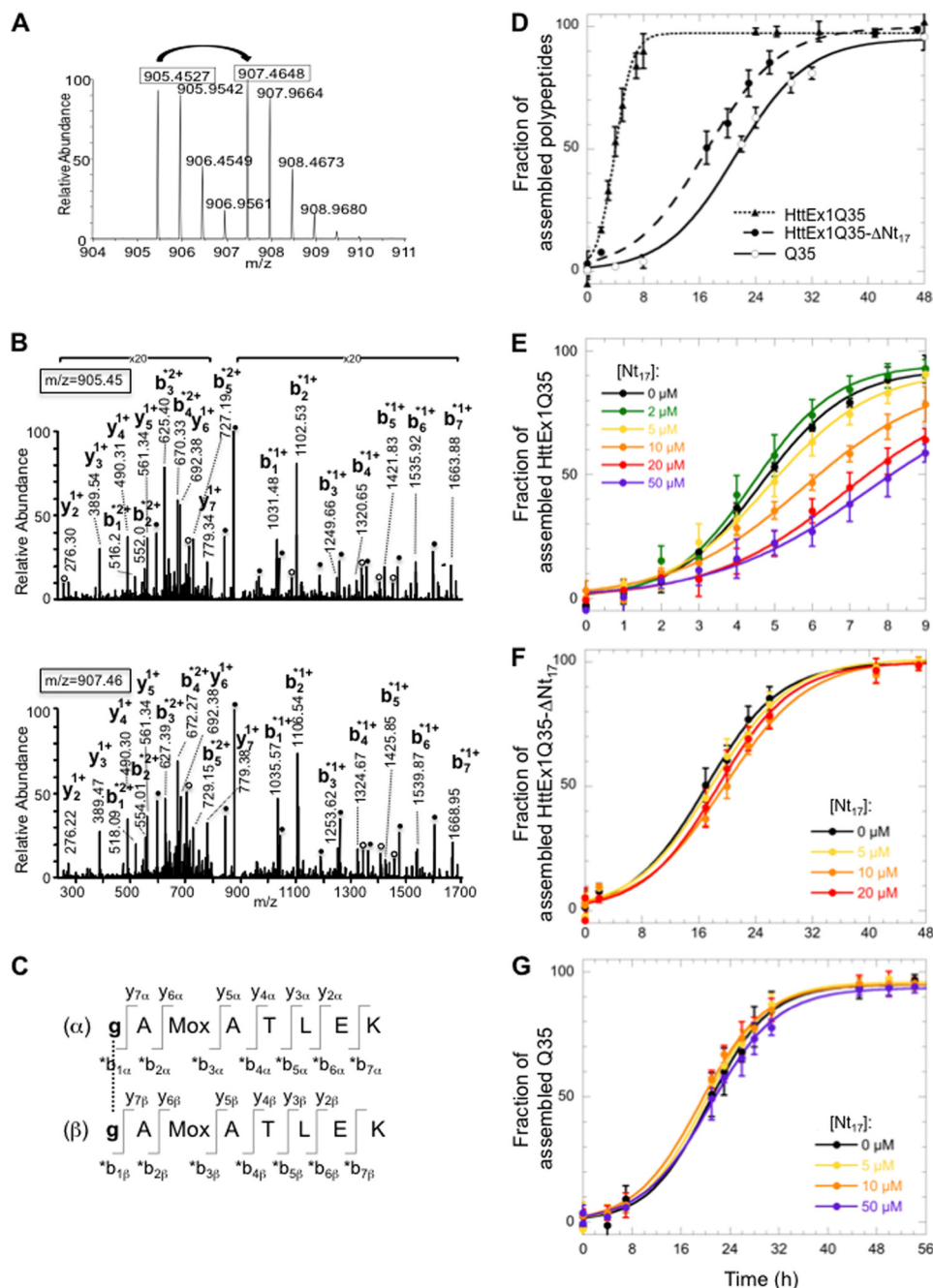


FIGURE 8. Role of the N-terminal flank in HttEx1Qn aggregation. *A*, mass spectrum of the double-charged Ex1Q25-Ex1Q25 cross-linked peptide with monoisotopic m/z 905.4527 and 907.4648 for the BS3-d0 and BS3-d4 peptides, respectively. *B*, LTQ-Orbitrap fragmentation mass spectra of the first isotope of the BS3-d0 peptide at m/z 905.45 (*top spectrum*) and the first isotope of the BS3-d4 peptide at m/z 907.46 (*bottom spectrum*). The identified fragments and their charge state are indicated. The *asterisks* indicate the fragments with the BS3-d0 or -d4 cross-linker. The *filled circles* indicate internal N-terminal fragments confirming the identified sequence, and the *empty circles* indicate fragment ions resulting from loss of water. Because both α and β sequences correspond to the same HttEx1Q25(1–8) sequence and generate identical α and β ion fragment masses, the α and β labels of the ion fragments annotation have been suppressed. *C*, the identified fragments are indicated on the HttEx1Q25 cross-linked sequences. The α and β sequences correspond to the two HttEx1Q25(1–8) peptides, respectively. This cross-link involves the N-terminal Gly-1 residue from two HttEx1Q25 molecules. *D*, time courses of HttEx1Q35, HttEx1Q35- Δ Nt₁₇, and Gln₃₅ (20 μ M each) assembly at 37 °C. *E–G*, time course of HttEx1Q35 (*E*), HttEx1Q35- Δ Nt₁₇ (*F*), and Gln₃₅ (*G*) (20 μ M each) assembly at 37 °C with increasing concentrations of free Nt₁₇. For all of the kinetics (*D–G*), each data point corresponds to the mean and associated S.E. calculated from 3–6 independent experiments.

peptides (11, 44), we show a strong exponential inverse correlation between the length of the polyQ stretch and the kinetics of HttEx1Qn aggregation, with no apparent threshold between pathological ($Q \geq 35$) and non-pathological ($Q \leq 30$) polyQ stretch lengths. The same exponential inverse correlation is observed between the length of huntingtin alleles ($Q \geq 40$) and

the age of onset of the disease (45–47), as if the kinetics of huntingtin aggregation would explain on its own the variations in the ages of onset. If this is indeed the case, one could speculate that short polyQ stretch lengths are non-pathological only because of our life span. By extrapolating the epidemic data from Wexler *et al.* (47) and considering a stretch of 17 Gln

residues (the most abundant allele in the human population), we conjecture that we would all develop HD if we lived for 145 years.

We sampled the SDS resistance of HttEx1Qn of different polyQ stretch lengths and saw differences between short and long polyQ stretches, as observed previously (48). Correspondingly, we observed a clear difference between the secondary structure content of fibrils formed by HttEx1Q25 and HttEx1Q48 as determined by FTIR, with the latter being richer in amyloid-like structures. Previously published structural analyses of polyQ fibrils performed mostly on synthetic polyQ showed no similar structural transition (49–51). However, one group reported differences in the FTIR spectra of fibrils from recombinant ataxin 3 containing 24 or 55 glutamines (52). The apparent discrepancy between results obtained using synthetic polyQ peptides and recombinant polyQ proteins highlights the importance of the natural context of polyQ stretches.

Finally, we note that the threshold we observed in the SDS resistance of the fibrils lies between 25 and 30 glutamines, when individuals carrying a huntingtin allele of less than 35 glutamines are considered healthy. One obvious explanation is that *in vitro* aggregation of recombinant polypeptides cannot recapitulate the whole toxic process that takes place in a living organism. However, recent studies show that individuals with intermediate polyQ lengths (*i.e.* 27–35 glutamines) display statistically significant clinical symptoms (53, 54), and cases of autopsy-proven HD with a polyQ stretch shorter than 30 have been reported (55, 56). The combination of these epidemiological data and our structural and kinetic results suggests that huntingtin alleles of intermediate polyQ lengths can indeed become pathological if an individual lives long enough.

Structure-Function Relationship for HttEx1Qn Fibrils—Hsc70, in its active, functional form, slows down HttEx1Qn assembly into fibrils. The resulting fibrils are indistinguishable from those obtained in the absence of Hsc70 based on electron micrographs. However, HttEx1Qn interaction with Hsc70 has effect on the fibrillar scaffold. HttEx1Qn fibrils assembled in the presence of Hsc70 have the secondary structure content and the functional properties of fibrils assembled from HttEx1Qn with non-pathological polyQ lengths. Our results establish a structure-function relationship for HttEx1Qn fibrils because different secondary structures of fibrils exhibit different infectious properties. We recently demonstrated that in the cases of both α -synuclein and HttEx1Qn, the fibrils are the most toxic species to the cells (57). Hence, the Hsc70-mediated changes in pathologic HttEx1Qn fibril structural and functional properties is of importance because it suggests that increased availability of Hsc70 *in vivo* may contribute to the clearance of fibrils and represent a therapeutic avenue.

A Detailed Mechanism of Action for Hsc70—We used a combination of different and complementary approaches to unveil the molecular mechanism by which Hsc70 mitigates HttEx1Qn aggregation. Multiple lines of evidence show that Hsc70 binds to the 17-residue-long N-terminal portion of the HttEx1Qn: (i) the effect of Hsc70 on HttEx1Qn aggregation does not depend on polyQ length but on the presence of the polyQ stretch N-terminal flank; (ii) Hsc70 binds fluorescently labeled free Nt₁₇; (iii)

free Nt₁₇ titrates the effect of Hsc70 on HttEx1Qn aggregation; and finally (iv) the residues involved in Hsc70-HttEx1Q25 interaction are all located in the HttEx1Q25 N-terminal flank, as revealed by our cross-linking studies. We cannot exclude the possibility that Hsc70 binds to another portion of the HttEx1Qn. This is, however, highly unlikely because we subjected Hsc70-HttEx1Qn to GluC digestion and detected no additional cross-links. There is currently no specific cross-linker that can react with a Gln residue, yet the fact that the Hsc70-HttEx1Qn interaction is independent of polyQ length while dependent on the HttEx1Qn N-terminal flank argues against a direct Hsc70-polyQ interaction.

Binding to a portion of the sequence or a domain adjacent to a polyQ tract may not be a prerogative of Hsc70. Hsp100 VCP, α B-crystallin (58, 59), TRiC, Ssa1, DnaJ, DnaK, or Hsp90 (42, 60–62) binds ataxin 3 or HttEx1Qn with normal or expanded polyQ stretch lengths in a similar way. However, to the best of our knowledge, this is the first time that a chaperone-binding site has been unequivocally mapped at a residue level precision to a flanking sequence of a polyQ-containing protein, allowing insight into the aggregation process of such proteins. This underlies the power and the potential of the cross-link-MS approach we developed previously (29, 63). In this respect, it is noteworthy that Hsc70 binds α -synuclein (29) and HttEx1Qn (this work) through the same residues within the substrate-binding domain. Other chaperones, such as DNAJB6, directly bind the polyQ tract because this chaperone has been shown to prevent the aggregation of polyQ much more efficiently than HttEx1Qn of the same polyQ length (64).

The N-terminal 17 Amino Acid Residues of HttEx1Qn and Aggregation—The findings that (i) HttEx1Qn aggregates faster than HttEx1Qn- Δ Nt₁₇, (ii) Nt₁₇ affects HttEx1Qn aggregation but not that of polyQ and HttEx1Qn- Δ Nt₁₇, and (iii) intermolecular Nt₁₇-Nt₁₇ interactions are established in the early stages of HttEx1Qn aggregation indicate that the Nt₁₇ flank of HttEx1Qn plays a critical role in the aggregation process.

Besides being involved in (i) cytosolic retention (35, 36), (ii) interaction with membranous structures (36, 38), and (iii) HD progression following post-translational modifications (35, 37, 65), the huntingtin Nt₁₇ flank seems to influence huntingtin aggregation. Studies aimed at documenting the exact role of the huntingtin Nt₁₇ flank have so far yielded contradictory observations. The effect of free Nt₁₇ on the aggregation of HttEx1Qn or a synthetic peptide almost reproducing HttEx1Qn had either antiaggregation (40, 41) or proaggregation (60) properties. In addition, Nt₁₇ either accelerated (60) or had effect on (40, 41) the aggregation of HttEx1Qn- Δ Nt₁₇. Our results unequivocally demonstrate that the HttEx1Qn N-terminal 17 amino acid residues play a critical role in HttEx1Qn assembly.

Two scenarios were proposed for the pathogenic aggregation of polyQ-containing proteins. In all cases, aggregation was proposed to be a two-step process. In a set of models, the polyQ stretch drives primarily aggregation, and the flanking regions have either countereffects or no effects (66, 67). In another set of models, it is the coalescence of polyQ stretch-flanking regions that drives the coalescence of the polyQ-containing proteins with secondary consolidation of the assemblies by the

Molecular Interaction between Hsc70 and Huntingtin Exon 1

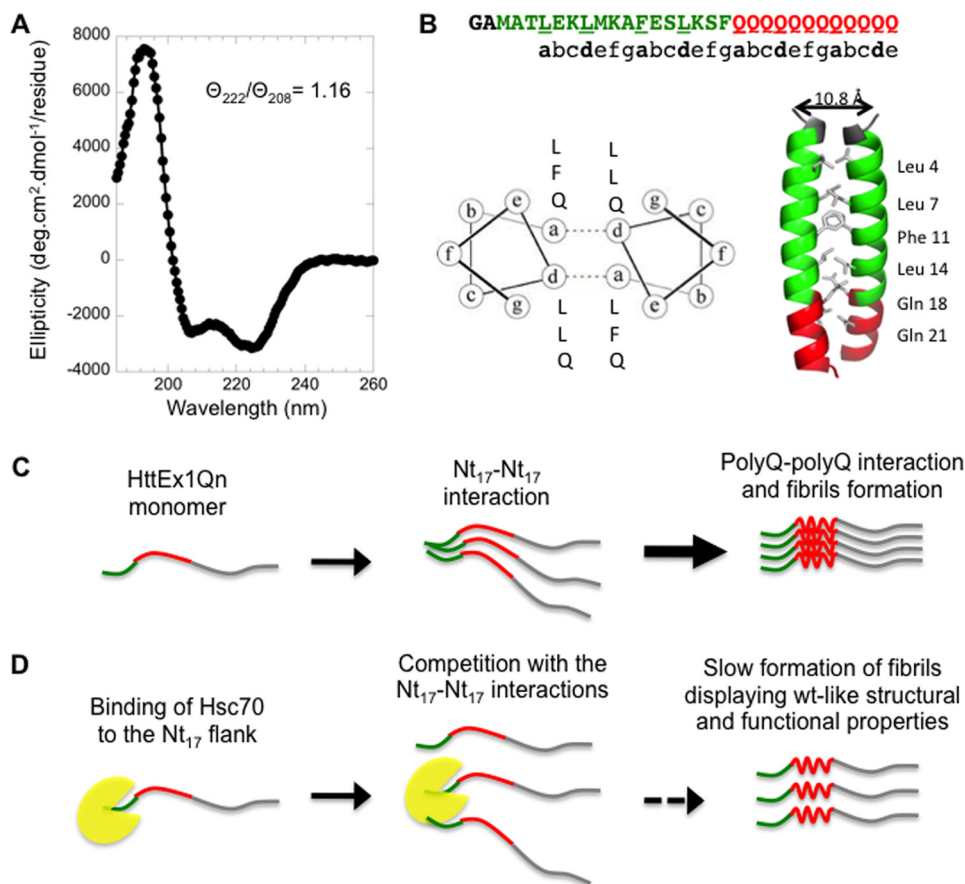


FIGURE 9. Model for HttEx1Qn aggregation and the effect of Hsc70. *A*, CD spectra of free Nt₁₇. The circular dichroism spectrum of the free Nt₁₇ peptide (2 mM) shows that it assembles into a coiled-coil quaternary structure ($\Theta_{222}/\Theta_{208} = 1.16$). *B*, the coiled-coil model for HttEx1Qn was built using the structure of the GCN4 leucine zipper coiled-coil (Protein Data Bank entry 2ZTA (70)). The Nt₁₇ sequence was aligned onto the GCN4 sequence to identify the leucine residues involved in the coiled-coil interaction. *C*, the two-step aggregation model of HttEx1Qn. HttEx1Qn coalescence is driven by homotypic interactions between the N-terminal flanks. PolyQ-polyQ interactions stabilize the nuclei and certainly contribute to fibril elongation at a later stage. *D*, mode of action of Hsc70. Hsc70 interferes with the aggregation process by interacting with the N-terminal flank, competing against the homotypic Nt₁₇-Nt₁₇ interactions and thus impeding the initial coalescence between HttEx1Qn molecules. The resulting fibrils differ in terms of structural and infectious properties.

rearrangement of the polyQ stretches into amyloid-like structures (68, 69). In the latter cases, further studies suggested that the polyQ stretch-flanking regions polymerize via the formation of coiled-coils (69). Our findings support the latter scenario with HttEx1Qn N-terminal flank-driven formation of in-register coiled-coils. Indeed we demonstrated that HttEx1Qn molecules are cross-linked early on during the assembly process through the N-terminal residue of their N-terminal flanks. In addition, free Nt₁₇ forms a coiled-coil structure in solution (Fig. 9A). Finally the cross-linker BS3, whose spacer arm length is 11 Å, imposes structural constraints indicative of the arrangement of HttEx1Qn molecules within on-assembly pathway HttEx1Qn oligomeric species. This in-register arrangement is schematized in Fig. 9B for the 17 N-terminal amino acid residues of HttEx1Qn in a wheel structural representation.

The overall contribution of the HttEx1Qn Nt₁₇ flank to the aggregation process and the interference of Hsc70 within the process is schematized in Fig. 9 (C and D). HttEx1Qn molecule coalescence, in the early stages of assembly, is driven by homotypic interactions between Nt₁₇ stretches. PolyQ-polyQ interactions stabilize the nuclei and certainly contribute to fibril elongation at a later stage (Fig. 9C). Hsc70 sequesters

HttEx1Qn molecules after binding their Nt₁₇ and interferes with HttEx1Qn coalescence. This impacts the kinetics of fibril formation. This also yields distinct HttEx1Qn folding intermediates, given that the resulting fibrils display lower β -sheet content, resistance to SDS, and nucleation/infectious propensities (Fig. 9D).

These modifications are likely to have biological relevance. By establishing the critical role of the 17 N-terminal amino acid residues of HttEx1Qn in its aggregation process, allowing insights into the geometry of the on-assembly pathway HttEx1Qn oligomeric species and identifying Hsc70 amino acid stretches that interact with HttEx1Qn, we lay the foundations of future therapeutic strategies. Indeed, the results we report pave the way for the design of therapeutic tools in HD targeting HttEx1Qn aggregation. Our findings may lead to the design of two classes of therapeutic tools: peptides derived from the N-terminal flank of HttEx1Qn that interfere with HttEx1Qn N-terminal flank-driven coalescence or peptides derived from the Hsc70 client protein binding site that interact with HttEx1Qn in a manner similar to the entire chaperone and (i) slow down aggregation and/or (ii) yield fibrils with limited resistance to the cellular clearance machinery and/or seeding propensity.

Acknowledgments—We thank Nils Maréchal, Laetitia Thomas, and Charlene Lasgi for experimental assistance. This work benefitted from the IMAGIF and Institut Curie imaging and sorting facilities and the mass spectrometry facility of the Centre de Recherche de Gif and Federative Research Institute Genomes, Transcriptomes, Proteomes.

REFERENCES

- Graham, R. K., Deng, Y., Slow, E. J., Haigh, B., Bissada, N., Lu, G., Pearson, J., Shehadeh, J., Bertram, L., Murphy, Z., Warby, S. C., Doty, C. N., Roy, S., Wellington, C. L., Leavitt, B. R., Raymond, L. A., Nicholson, D. W., and Hayden, M. R. (2006) Cleavage at the caspase-6 site is required for neuronal dysfunction and degeneration due to mutant huntingtin. *Cell* **125**, 1179–1191
- Sieradzan, K. A., Mehan, A. O., Jones, L., Wanker, E. E., Nukina, N., and Mann, D. M. (1999) Huntingtin's disease intranuclear inclusions contain truncated, ubiquitinated huntingtin protein. *Exp. Neurol.* **156**, 92–99
- DiFiglia, M., Sapp, E., Chase, K. O., Davies, S. W., Bates, G. P., Vonsattel, J. P., and Aronin, N. (1997) Aggregation of huntingtin in neuronal intranuclear inclusions and dystrophic neurites in brain. *Science* **277**, 1990–1993
- Schulte, J., and Littleton, J. T. (2011) The biological function of the Huntingtin protein and its relevance to Huntington's disease pathology. *Curr. Trends Neurol.* **5**, 65–78
- Paulson, H. L., Bonini, N. M., and Roth, K. A. (2000) Polyglutamine disease and neuronal cell death. *Proc. Natl. Acad. Sci. U.S.A.* **97**, 12957–12958
- Finkbeiner, S. (2011) Huntington's disease. *Cold Spring Harb. Perspect. Biol.* **10**.1101/cshperspect.a007476
- Rubinsztein, D. C. (2002) Lessons from animal models of Huntington's disease. *Trends Genet.* **18**, 202–209
- Scherzinger, E., Sittler, A., Schweiger, K., Heiser, V., Lurz, R., Hasenbank, R., Bates, G. P., Lehrach, H., and Wanker, E. E. (1999) Self-assembly of polyglutamine-containing huntingtin fragments into amyloid-like fibrils: implications for Huntington's disease pathology. *Proc. Natl. Acad. Sci. U.S.A.* **96**, 4604–4609
- Brundin, P., Melki, R., and Kopito, R. (2010) Prion-like transmission of protein aggregates in neurodegenerative diseases. *Nat. Rev. Mol. Cell Biol.* **11**, 301–307
- Ren, P.-H., Lauckner, J. E., Kachirskaia, I., Heuser, J. E., Melki, R., and Kopito, R. R. (2009) Cytoplasmic penetration and persistent infection of mammalian cells by polyglutamine aggregates. *Nat. Cell Biol.* **11**, 219–225
- Chen, S., Berthelie, V., Yang, W., and Wetzel, R. (2001) Polyglutamine aggregation behavior *in vitro* supports a recruitment mechanism of cytotoxicity. *J. Mol. Biol.* **311**, 173–182
- Bhattacharyya, A., Thakur, A. K., Chellgren, V. M., Thiagarajan, G., Williams, A. D., Chellgren, B. W., Creamer, T. P., and Wetzel, R. (2006) Oligoproline effects on polyglutamine conformation and aggregation. *J. Mol. Biol.* **355**, 524–535
- Sivanandam, V. N., Jayaraman, M., Hoop, C. L., Kodali, R., Wetzel, R., and van der Wel, P. C. A. (2011) The aggregation-enhancing huntingtin N-terminus is helical in amyloid fibrils. *J. Am. Chem. Soc.* **133**, 4558–4566
- Kelley, N. W., Huang, X., Tam, S., Spiess, C., Frydman, J., and Pande, V. S. (2009) The predicted structure of the headpiece of the huntingtin protein and its implications on huntingtin aggregation. *J. Mol. Biol.* **388**, 919–927
- Rujano, M. A., Kampinga, H. H., and Salomons, F. A. (2007) Modulation of polyglutamine inclusion formation by the Hsp70 chaperone machine. *Exp. Cell Res.* **313**, 3568–3578
- Hay, D. G., Sathasivam, K., Tobaben, S., Stahl, B., Marber, M., Mestril, R., Mahal, A., Smith, D. L., Woodman, B., and Bates, G. P. (2004) Progressive decrease in chaperone protein levels in a mouse model of Huntington's disease and induction of stress proteins as a therapeutic approach. *Hum. Mol. Genet.* **13**, 1389–1405
- Tagawa, K., Marubuchi, S., Qi, M.-L., Enokido, Y., Tamura, T., Inagaki, R., Murata, M., Kanazawa, I., Wanker, E. E., and Okazawa, H. (2007) The induction levels of heat shock protein 70 differentiate the vulnerabilities to mutant huntingtin among neuronal subtypes. *J. Neurosci.* **27**, 868–880
- Chan, H. Y., Warrick, J. M., Gray-Board, G. L., Paulson, H. L., and Bonini, N. M. (2000) Mechanisms of chaperone suppression of polyglutamine disease: selectivity, synergy and modulation of protein solubility in *Drosophila*. *Hum. Mol. Genet.* **9**, 2811–2820
- Olshina, M. A., Angley, L. M., Ramdzan, Y. M., Tang, J., Bailey, M. F., Hill, A. F., and Hatters, D. M. (2010) Tracking mutant huntingtin aggregation kinetics in cells reveals three major populations that include an invariant oligomer pool. *J. Biol. Chem.* **285**, 21807–21816
- Zhou, H., Li, S. H., and Li, X. J. (2001) Chaperone suppression of cellular toxicity of huntingtin is independent of polyglutamine aggregation. *J. Biol. Chem.* **276**, 48417–48424
- Meriin, A. B., Zhang, X., He, X., Newnam, G. P., Chernoff, Y. O., and Sherman, M. Y. (2002) Huntingtin toxicity in yeast model depends on polyglutamine aggregation mediated by a prion-like protein Rnq1. *J. Cell Biol.* **157**, 997–1004
- Yu, A., Shibata, Y., Shah, B., Calamini, B., Lo, D. C., and Morimoto, R. I. (2014) Protein aggregation can inhibit clathrin-mediated endocytosis by chaperone competition. *Proc. Natl. Acad. Sci. U.S.A.* **111**, E1481–E1490
- Rüdiger, S., Germeroth, L., Schneider-Mergener, J., and Bukau, B. (1997) Substrate specificity of the DnaK chaperone determined by screening cellulose-bound peptide libraries. *EMBO J.* **16**, 1501–1507
- Rüdiger, S., Schneider-Mergener, J., and Bukau, B. (2001) Its substrate specificity characterizes the DnaJ co-chaperone as a scanning factor for the DnaK chaperone. *EMBO J.* **20**, 1042–1050
- Pemberton, S., Madiona, K., Pieri, L., Kabani, M., Bousset, L., and Melki, R. (2011) Hsc70 protein interaction with soluble and fibrillar α -synuclein. *J. Biol. Chem.* **286**, 34690–34699
- Wanker, E. E., Scherzinger, E., Heiser, V., Sittler, A., Eickhoff, H., and Lehrach, H. (1999) Membrane filter assay for detection of amyloid-like polyglutamine-containing protein aggregates. *Methods Enzymol.* **309**, 375–386
- Zurdo, J., Guijarro, J. I., and Dobson, C. M. (2001) Preparation and characterization of purified amyloid fibrils. *J. Am. Chem. Soc.* **123**, 8141–8142
- Seshadri, S., Khurana, R., and Fink, A. L. (1999) Fourier transform infrared spectroscopy in analysis of protein deposits. *Methods Enzymol.* **309**, 559–576
- Redeker, V., Pemberton, S., Bienvenut, W., Bousset, L., and Melki, R. (2012) Identification of protein interfaces between α -synuclein, the principal component of Lewy bodies in Parkinson disease, and the molecular chaperones human Hsc70 and the yeast Ssa1p. *J. Biol. Chem.* **287**, 32630–32639
- Mädler, S., Bich, C., Touboul, D., and Zenobi, R. (2009) Chemical cross-linking with NHS esters: a systematic study on amino acid reactivities. *J. Mass Spectrom.* **44**, 694–706
- Zimmer, J. S. D., Monroe, M. E., Qian, W. J., and Smith, R. D. (2006) Advances in proteomics data analysis and display using an accurate mass and time tag approach. *Mass Spectrom. Rev.* **25**, 450–482
- Peri, S., Steen, H., and Pandey, A. (2001) GPMAW: a software tool for analyzing proteins and peptides. *Trends Biochem. Sci.* **26**, 687–689
- Rinner, O., Seebacher, J., Walzthoeni, T., Mueller, L. N., Beck, M., Schmidt, A., Mueller, M., and Aebersold, R. (2008) Identification of cross-linked peptides from large sequence databases. *Nat. Methods* **5**, 315–318
- Trevino, R. S., Lauckner, J. E., Sourigues, Y., Pearce, M. M., Bousset, L., Melki, R., and Kopito, R. R. (2012) Fibrillar structure and charge determine the interaction of polyglutamine protein aggregates with the cell surface. *J. Biol. Chem.* **287**, 29722–29728
- Steffan, J. S., Agrawal, N., Pallos, J., Rockabrand, E., Trotman, L. C., Slepko, N., Illes, K., Lukacsovich, T., Zhu, Y.-Z., Cattaneo, E., Pandolfi, P. P., Thompson, L. M., and Marsh, J. L. (2004) SUMO modification of Huntingtin and Huntington's disease pathology. *Science* **304**, 100–104
- Atwal, R. S., Xia, J., Pinchev, D., Taylor, J., Epan, R. M., and Truant, R. (2007) Huntingtin has a membrane association signal that can modulate huntingtin aggregation, nuclear entry and toxicity. *Hum. Mol. Genet.* **16**, 2600–2615
- Atwal, R. S., Desmond, C. R., Caron, N., Maiuri, T., Xia, J., Sipione, S., and Truant, R. (2011) Kinase inhibitors modulate huntingtin cell localization and toxicity. *Nat. Chem. Biol.* **7**, 453–460
- Rockabrand, E., Slepko, N., Pantalone, A., Nukala, V. N., Kazantsev, A., Marsh, J. L., Sullivan, P. G., Steffan, J. S., Sensi, S. L., and Thompson, L. M. (2007) The first 17 amino acids of Huntingtin modulate its sub-cellular

Molecular Interaction between Hsc70 and Huntingtin Exon 1

- localization, aggregation and effects on calcium homeostasis. *Hum. Mol. Genet.* **16**, 61–77
39. Wetzel, R. (2012) Physical chemistry of polyglutamine: intriguing tales of a monotonous sequence. *J. Mol. Biol.* **421**, 466–490
40. Mishra, R., Jayaraman, M., Roland, B. P., Landrum, E., Fullam, T., Kodali, R., Thakur, A. K., Arduini, I., and Wetzel, R. (2012) Inhibiting the nucleation of amyloid structure in a huntingtin fragment by targeting α -helix-rich oligomeric intermediates. *J. Mol. Biol.* **415**, 900–917
41. Jayaraman, M., Mishra, R., Kodali, R., Thakur, A. K., Koharudin, L. M. I., Gronenborn, A. M., and Wetzel, R. (2012) Kinetically competing huntingtin aggregation pathways control amyloid polymorphism and properties. *Biochemistry* **51**, 2706–2716
42. Muchowski, P. J., Schaffar, G., Sittler, A., Wanker, E. E., Hayer-Hartl, M. K., and Hartl, F. U. (2000) Hsp70 and hsp40 chaperones can inhibit self-assembly of polyglutamine proteins into amyloid-like fibrils. *Proc. Natl. Acad. Sci. U.S.A.* **97**, 7841–7846
43. Guzhova, I. V., Lazarev, V. F., Kaznacheeva, A. V., Ippolitova, M. V., Muronetz, V. I., Kinev, A. V., and Margulis, B. A. (2011) Novel mechanism of Hsp70 chaperone-mediated prevention of polyglutamine aggregates in a cellular model of huntington disease. *Hum. Mol. Genet.* **20**, 3953–3963
44. Landrum, E., and Wetzel, R. (2014) Biophysical underpinnings of the repeat length dependence of polyglutamine amyloid formation. *J. Biol. Chem.* **289**, 10254–10260
45. Andrew, S. E., Goldberg, Y. P., Kremer, B., Telenius, H., Theilmann, J., Adam, S., Starr, E., Squitieri, F., Lin, B., and Kalchman, M. A. (1993) The relationship between trinucleotide (CAG) repeat length and clinical features of Huntington's disease. *Nat. Genet.* **4**, 398–403
46. Brinkman, R. R., Mezei, M. M., Theilmann, J., Almqvist, E., and Hayden, M. R. (1997) The likelihood of being affected with Huntington disease by a particular age, for a specific CAG size. *Am. J. Hum. Genet.* **60**, 1202–1210
47. Wexler, N. S., Lorimer, J., Porter, J., Gomez, F., Moskowitz, C., Shackell, E., Marder, K., Penchaszadeh, G., Roberts, S. A., Gayán, J., Brocklebank, D., Cherny, S. S., Cardon, L. R., Gray, J., Dlouhy, S. R., Wiktorski, S., Hodes, M. E., Conneally, P. M., Penney, J. B., Gusella, J., Cha, J.-H., Irizarry, M., Rosas, D., Hersch, S., Hollingsworth, Z., MacDonald, M., Young, A. B., Andresen, J. M., Housman, D. E., De Young, M. M., Bonilla, E., Stillings, T., Negrette, A., Snodgrass, S. R., Martinez-Jaurrieta, M. D., Ramos-Arroyo, M. A., Bickham, J., Ramos, J. S., Marshall, F., Shoulson, I., Rey, G. J., Feigin, A., Arnheim, N., Acevedo-Cruz, A., Acosta, L., Alvir, J., Fischbeck, K., Thompson, L. M., Young, A., Dure, L., O'Brien, C. J., Paulsen, J., Brickman, A., Krch, D., Peery, S., Hogarth, P., Higgins, D. S., and Landwehrmeyer, B. (2004) Venezuelan kindreds reveal that genetic and environmental factors modulate Huntington's disease age of onset. *Proc. Natl. Acad. Sci. U.S.A.* **101**, 3498–3503
48. Klein, F. A. C., Pastore, A., Masino, L., Zeder-Lutz, G., Nierengarten, H., Oulad-Abdelghani, M., Altschuh, D., Mandel, J. L., and Trotter, Y. (2007) Pathogenic and non-pathogenic polyglutamine tracts have similar structural properties: towards a length-dependent toxicity gradient. *J. Mol. Biol.* **371**, 235–244
49. Thakur, A. K., Jayaraman, M., Mishra, R., Thakur, M., Chellgren, V. M., Byeon, I.-J. L., Anjum, D. H., Kodali, R., Creamer, T. P., Conway, J. F., Gronenborn, A. M., and Wetzel, R. (2009) Polyglutamine disruption of the huntingtin exon 1 N terminus triggers a complex aggregation mechanism. *Nat. Struct. Mol. Biol.* **16**, 380–389
50. Sharma, D., Shinchuk, L. M., Inouye, H., Wetzel, R., and Kirschner, D. A. (2005) Polyglutamine homopolymers having 8–45 residues form slablike β -crystallite assemblies. *Proteins* **61**, 398–411
51. Kurouski, D., Kar, K., Wetzel, R., Dukor, R. K., Lednev, I. K., and Nafie, L. A. (2013) Levels of supramolecular chirality of polyglutamine aggregates revealed by vibrational circular dichroism. *FEBS Lett.* **587**, 1638–1643
52. Natalello, A., Frana, A. M., Relini, A., Apicella, A., Invernizzi, G., Casari, C., Gliozzi, A., Doglia, S. M., Tortora, P., and Regonesi, M. E. (2011) A major role for side-chain polyglutamine hydrogen bonding in irreversible ataxin-3 aggregation. *PLoS One* **6**, e18789
53. Ha, A. D., and Jankovic, J. (2011) Exploring the correlates of intermediate CAG repeats in Huntington disease. *Postgrad. Med.* **123**, 116–121
54. Killoran, A., Biglan, K. M., Jankovic, J., Eberly, S., Kayson, E., Oakes, D., Young, A. B., and Shoulson, I. (2013) Characterization of the Huntington intermediate CAG repeat expansion phenotype in PHAROS. *Neurology* **80**, 2022–2027
55. Kenney, C., Powell, S., and Jankovic, J. (2007) Autopsy-proven Huntington's disease with 29 trinucleotide repeats. *Mov. Disord.* **22**, 127–130
56. Groen, J. L., de Bie, R. M. A., Foncke, E. M. J., Roos, R. A. C., Leenders, K. L., and Tijssen, M. A. J. (2010) Late-onset Huntington disease with intermediate CAG repeats: true or false? *J. Neurol. Neurosurg. Psychiatry* **81**, 228–230
57. Pieri, L., Madiona, K., Bousset, L., and Melki, R. (2012) Fibrillar α -synuclein and huntingtin exon 1 assemblies are toxic to the cells. *Biophys. J.* **102**, 2894–2905
58. Boeddrich, A., Gaumer, S., Haacke, A., Tzvetkov, N., Albrecht, M., Evert, B. O., Müller, E. C., Lurz, R., Breuer, P., Schugardt, N., Plassmann, S., Xu, K., Warrick, J. M., Suopanki, J., Wüllner, U., Frank, R., Hartl, U. F., Bonini, N. M., and Wanker, E. E. (2006) An arginine/lysine-rich motif is crucial for VCP/p97-mediated modulation of ataxin-3 fibrillogenesis. *EMBO J.* **25**, 1547–1558
59. Robertson, A. L., Headey, S. J., Saunders, H. M., Ecroyd, H., Scanlon, M. J., Carver, J. A., and Bottomley, S. P. (2010) Small heat-shock proteins interact with a flanking domain to suppress polyglutamine aggregation. *Proc. Natl. Acad. Sci. U.S.A.* **107**, 10424–10429
60. Tam, S., Spiess, C., Auyeung, W., Joachimiak, L., Chen, B., Poirier, M. A., and Frydman, J. (2009) The chaperonin TRiC blocks a huntingtin sequence element that promotes the conformational switch to aggregation. *Nat. Struct. Mol. Biol.* **16**, 1279–1285
61. Tam, S., Geller, R., Spiess, C., and Frydman, J. (2006) The chaperonin TRiC controls polyglutamine aggregation and toxicity through subunit-specific interactions. *Nat. Cell Biol.* **8**, 1155–1162
62. Baldo, B., Weiss, A., Parker, C. N., Bibel, M., Paganetti, P., and Kaupmann, K. (2012) A screen for enhancers of clearance identifies huntingtin as a heat shock protein 90 (Hsp90) client protein. *J. Biol. Chem.* **287**, 1406–1414
63. Redeker, V., Bonnefoy, J., Le Caer, J.-P., Pemberton, S., Laprèvote, O., and Melki, R. (2010) A region within the C-terminal domain of Ure2p is shown to interact with the molecular chaperone Ssa1p by the use of cross-linkers and mass spectrometry. *FEBS J.* **277**, 5112–5123
64. Månsson, C., Kakkar, V., Monsellier, E., Sourigues, Y., Härmärk, J., Kampinga, H. H., Melki, R., and Emanuelsson, C. (2014) DNAJB6 is a peptide-binding chaperone which can suppress amyloid fibrillation of polyglutamine peptides at substoichiometric molar ratios. *Cell Stress Chaperones* **19**, 227–239
65. Gu, X., Greiner, E. R., Mishra, R., Kodali, R., Osmand, A., Finkbeiner, S., Steffan, J. S., Thompson, L. M., Wetzel, R., and Yang, X. W. (2009) Serines 13 and 16 are critical determinants of full-length human mutant huntingtin induced disease pathogenesis in HD mice. *Neuron* **64**, 828–840
66. Robertson, A. L., Horne, J., Ellsion, A. M., Thomas, B., Scanlon, M. J., and Bottomley, S. P. (2008) The structural impact of a polyglutamine tract is location-dependent. *Biophys. J.* **95**, 5922–5930
67. Darnell, G., Orgel, J. P. R. O., Pahl, R., and Meredith, S. C. (2007) Flanking polyproline sequences inhibit beta-sheet structure in polyglutamine segments by inducing PPII-like helix structure. *J. Mol. Biol.* **374**, 688–704
68. Ellsion, A. M., Thomas, B., and Bottomley, S. P. (2006) The two-stage pathway of ataxin-3 fibrillogenesis involves a polyglutamine-independent step. *J. Biol. Chem.* **281**, 16888–16896
69. Fiumara, F., Fioriti, L., Kandel, E. R., and Hendrickson, W. A. (2010) Essential role of coiled coils for aggregation and activity of Q/N-rich prions and PolyQ proteins. *Cell* **143**, 1121–1135
70. O'Shea, E. K., Klemm, J. D., Kim, P. S., and Alber, T. (1991) X-ray structure of the GCN4 leucine zipper, a two-stranded, parallel coiled coil. *Science* **254**, 539–544